1-1-1983

Magnetite - franklinite - pyrophanite intergrowths of the Sterling Hill zinc deposit, Sussex County, New Jersey: An analytical and experimental study.

Albert J. Valentino

MAGNETITE - FRANKLINITE - PYROPHANITE INTERGROWTHS OF THE STERLING HILL ZINC DEPOSIT, SUSSEX COUNTY, NEW JERSEY: AN ANALYTICAL AND EXPERIMENTAL STUDY

by

Albert J. Valentino

A Thesis

Presented to the Graduate Committee

of Lehigh University

in Candidacy for the Degree of

Master of Science

in

Geology

Lehigh University

1983

MAGNETITE - FRANKLINITE - PYROPHANITE INTERGROWTHS OF THE STERLING HILL ZINC DEPOSIT, SUSSEX COUNTY, NEW JERSEY: AN ANALYTICAL AND EXPERIMENTAL STUDY

by

Albert J. Valentino

A Thesis

Presented to the Graduate Committee

of Lehigh University

in Candidacy for the Degree of

Master of Science

in

Geology

Lehigh University

1983

This thesis is accepted and approved in partial fulfillment of the requirements for the degree of Master of Science.

April 7, 1983
(date)

Professor in Charge

Chairman of Department

ABSTRACT

The Sterling Hill zinc deposit is a regionally metamorphosed stratiform oxide-silicate deposit enclosed in the Precambrian Grenville marble belt of the New Jersey Highlands. Within this deposit are oriented exsolution intergrowths of magnetite (ideally $FeFe_2O_4$) and franklinite (ideally $ZnFe_2O_4$) whose bulk chemistry ranges from Mag_{55} to Mag_{65}. These intergrowths represent a once homogeneous spinel phase and indicate the presence of a solvus in system $FeFe_2O_4$ - $ZnFe_2O_4$. The primary objective of this study was to determine experimentally the solvus in this system and to integrate these sub-solidus phase relations with the composition of naturally occurring magnetite-franklinite exsolution intergrowths. The composition of the latter was determined with the electron microprobe to develop a new spinel geothermometer and to ascertain a minimum peak temperature of the regional metamorphic event which produced this deposit.

A series of reversible hydrothermal experiments were carried out in the system $FeFe_2O_4$ - $ZnFe_2O_4$ at 0.1 GPa water pressure in the temperature range of 400-900°C for periods of 5-104 days to determine the miscibility gap. The reactants used were high-purity synthetic homogeneous spinels of composition Mag_{50} and a equimolar mechanical mixture of Mag_{90} and Mag_{10} (bulk composition Mag_{51}). All of these synthetic spinels used in the hydrothermal

experiments were synthesized in a gas-mixing furnace under flowing CO_2 at 1200°C. Products of these hydrothermal experiments were characterized by X-ray powder diffractometry using CuKα and FeKα radiation. The results show that the consolute temperature of the solvus must lie below 500°C and may be at or below 400°C. These results also indicate that unmixing of magnetite-franklinite solid solution must have taken place at or below this temperature and that the solvus is too low in temperature to be useful as a geothermometer.

One set of magnetite-franklinite intergrowths contains rhombohedral exsolution lamellae in the (111) plane of the magnetite-rich lamellae which are up to 1 μm wide and 10 μm long. Results of electron microprobe analysis of this phase, elemental X-ray maps, and atomic number contrast from backscattered electron images as well as its textural occurrence indicate that this phase is pyrophanite ($MnTiO_3$). The presence of this phase indicates that during the first unmixing Mn and Ti selectively partitioned into the magnetite-rich lamellae. Upon further cooling a second unmixing event took place in the Mn-Ti-rich magnetite resulting in lamellae of the rhombohedral phase pyrophanite parallel to the (111) planes of the magnetite host. This occurrence of pyrophanite was not known to occur in the Franklin-Sterling Hill district before this study and therefore constitutes the 287th mineral found at this remarkable locality.

ACKNOWLEDGMENTS

I wish to thank the efforts of my thesis adviser, Dr. Charles B. Sclar, who greatly inspired this study and for his critical review of this manuscript. I would also like to thank the other members of my committee for their help, Dr. Paul B. Myers of the Department of Geological Sciences at Lehigh University and Mr. Robert W. Metsger, Chief Geologist of the New Jersey Zinc Company. Mr. Metsger was especially helpful with the supervision of sample collection for this study.

I would like to thank Dr. Donald H. Lindsley of the Department of Earth and Space Sciences at the State University of New York at Stony Brook. Dr. Lindsley educated me in the science of hydrothermal experimentation and kindly made available his hydrothermal facilities where the initial hydrothermal work was carried out.

Financial support for this study was partly defrayed by a Grant-in-Aid from Sigma Xi, the Scientific Research Society of North America. Personal financial support was partly defrayed by the Department of Geological Sciences who graciously awarded me a graduate teaching assistantship from 1980 through 1982.

A special thanks to Mr. James E. Kerner, electron microprobe technician in the Department of Metallurgy and Materials Engineering at Lehigh University who bent over backwards to instruct me on and get access to the electron microprobe.

Lastly, I would like to thank the men of 541 Seneca Street, Apt. IC, better known as In-Crowd for their continuous and well needed friendship throughout the course of this study. They are: Steve (The Wick) Siwiec, Phil (The Boy) Lagas, Jim (Bloom) Bloomfield, Bob (The Fella) Gallagher, Jim (Zigs) Zigmont, and Alan (Allione) Benimoff.

TABLE OF CONTENTS

TABLE OF CONTENTS (cont.)

LIST OF FIGURES

LIST OF FIGURES

LIST OF FIGURES (cont.)

LIST OF TABLES

INTRODUCTION

The Sterling Hill zinc deposit, which is enclosed in the Precambrian Grenville marble of the New Jersey Highlands, is one of a pair of mineralogically unique ore deposits. The other is the Franklin ore body which appears to be genetically related to the Sterling Hill deposit. Both deposits have the following characteristics in common; 1) a host rock of folded Precambrian Franklin marble, 2) a synclinal structure which plunges northeast, 3) the three-fold association of iron, zinc, and manganese which is unique in mineralized zones of economic size, 4) identical major mineralogy with respect to the ore minerals of zinc, and 5) mineralogical layering parallel to structure (Metsger, et al., 1958). These deposits are remarkable because the common ore minerals of zinc are either sphalerite (ZnS), or smithsonite ($ZnCO_3$) both of which are virtually absent at Sterling Hill and Franklin. Instead, the pricipal ore minerals are oxides and silicates of zinc, namely, franklinite [$(Zn,Mn,Fe^{+2})(Fe^{+3},Mn)_2O_4$], zincite (ZnO), and willemite (Zn_2SiO_4), which apparently constitute, along with the calcite of the host marble, a metamorphic assemblage.

The Franklin ore body is well known to mineral collectors because of the occurrence of over 250 mineral species, several of which are known only from Franklin. However, the

mineralogy of the Sterling Hill deposit is relatively simple. The Franklin deposit apparently was overprinted with a large variety of minerals of hydrothermal origin which obscure many important primary genetic relationships. Therefore, the Sterling Hill ore body is much more promising for detailed study with respect to understanding the metamorphic event which produced these deposits as well as the pre-metamorphic sedimentary environment and the mineralogical distribution of iron, zinc, and manganese.

OBJECTIVES

Previous literature on the Sterling Hill and Franklin ore bodies can be grouped into four classes; 1) the descriptive mineralogy of the unique mineral assemblage, 2) the complex structure of these stratiform zinc deposits, 3) the origin of the deposits, and 4) quantitative studies of the physical conditions of metamorphism such as temperature and pressure. The purpose of this investigation was to contribute to (4), the physical conditions of metamorphism. The primary objectives were the development of a new spinel geothermometer and the determination of the minimum peak temperature of regional metamorphism at Sterling Hill by means of this new geothermometer. This geothermometer was to be based on 1) the

position and shape of the miscibility gap for the ideal binary system magnetite ($FeFe_2O_4$)-franklinite ($ZnFe_2O_4$), which was to be experimentally determined in this study, and 2) the bulk composition of naturally occurring exsolution intergrowths of magnetite and franklinite, which were collected from known locations in the Sterling Hill mine. These magnetite-franklinite exsolution intergrowths represent a once homogeneous spinel phase which exsolved during cooling topotactically parallel to the cube face (100), into oriented intergrowths of two spinels, namely, magnetite-rich solid solution and franklinite-rich solid solution. The homogenization temperatures for each of these intergrowths would represent a minimum temperature attained during regional metamorphism at Sterling Hill.

Some of the magnetite lamellae of the naturally occurring magnetite-franklinite exsolution intergrowths contain a second set of minute exsolution lamellae. This second set is non-cubic as evidenced by its optically anisotropic character and appears to be oriented parallel to the (111) plane of the magnetite host. The lamellae are no more than 1μm wide and 10μm long. Thus, a second objective of this study was the assessment of the structure, chemistry, and the origin of this phase based on its textural relations and electron microprobe

analysis complemented by atomic-number contrast from backscattered electron imaging and elemental X-ray mapping.

PREVIOUS INVESTIGATIONS

Many theories have been proposed for the origin of the Sterling Hill zinc deposit. These ideas range from a metasomatic (hydrothermal-igneous) origin (Ridge, 1952; Takahashi and Myers, 1963) to a syngenetic origin (Frondel and Baum, 1974; Squiller, 1976; Squiller and Sclar, 1980). In the latter view, iron, zinc, and manganese at Sterling Hill may have been expressed mineralogically in the original impure siliceous ferruginous carbonate mud as a ferroan-zincian-manganoan dolomite intimately mixed with silica gel and very fine-grained iron and manganese oxides. Subsequent deep-seated high-rank regional metamorphism would give rise through the dedolomitization reaction to impure zinc oxide, solid solution, calcite solid solution, and CO_2. In turn, the zinc oxide would have reacted with the contiguous silica and/or oxides of iron and manganese to yield willemite and franklinite, respectively. The present ore minerals can be explained through local metamorphic reactions on a volume scale of .05-5 cm^3 as follows: 1) franklinite developed where oxides with a high Fe/Mn ratio were present and silica gel was absent, 2) willemite developed where silica gel was present

and oxides of iron and manganese were virtually absent, and 3) zincite remained where both silica gel and iron and manganese oxides were absent.

Frondel and Klein (1965) determined the minimum peak temperature of regional metamorphism to be between 650-700°C based on naturally occurring hetaerolite-franklinite exsolution intergrowths and the equilibrium diagrams of Mason (1947) for the system Fe_3O_4-Mn_3O_4-$ZnMn_2O_4$-$ZnFe_2O_4$. Carvalho (1978) raised the minimum peak temperature to 760±50°C based on the bulk composition of naturally occurring gahnite-franklinite exsolution intergrowths and their experimentally determined solvus loop in the ideal binary system gahnite ($ZnAl_2O_4$)-franklinite ($ZnFe_2O_4$). These temperatures should have been high enough to dedolomitize the hypothetical primary zincian dolomite.

THE STERLING HILL ZINC DEPOSIT

Geologic Setting

The Franklin-Sterling Hill deposits are located on the northwestern edge of the New Jersey Highlands (Fig. 1). Both the Franklin and Sterling Hill deposits are enclosed in the Franklin marble which is a member of a series of Precambrian metasedimentary rocks that were intensely folded and

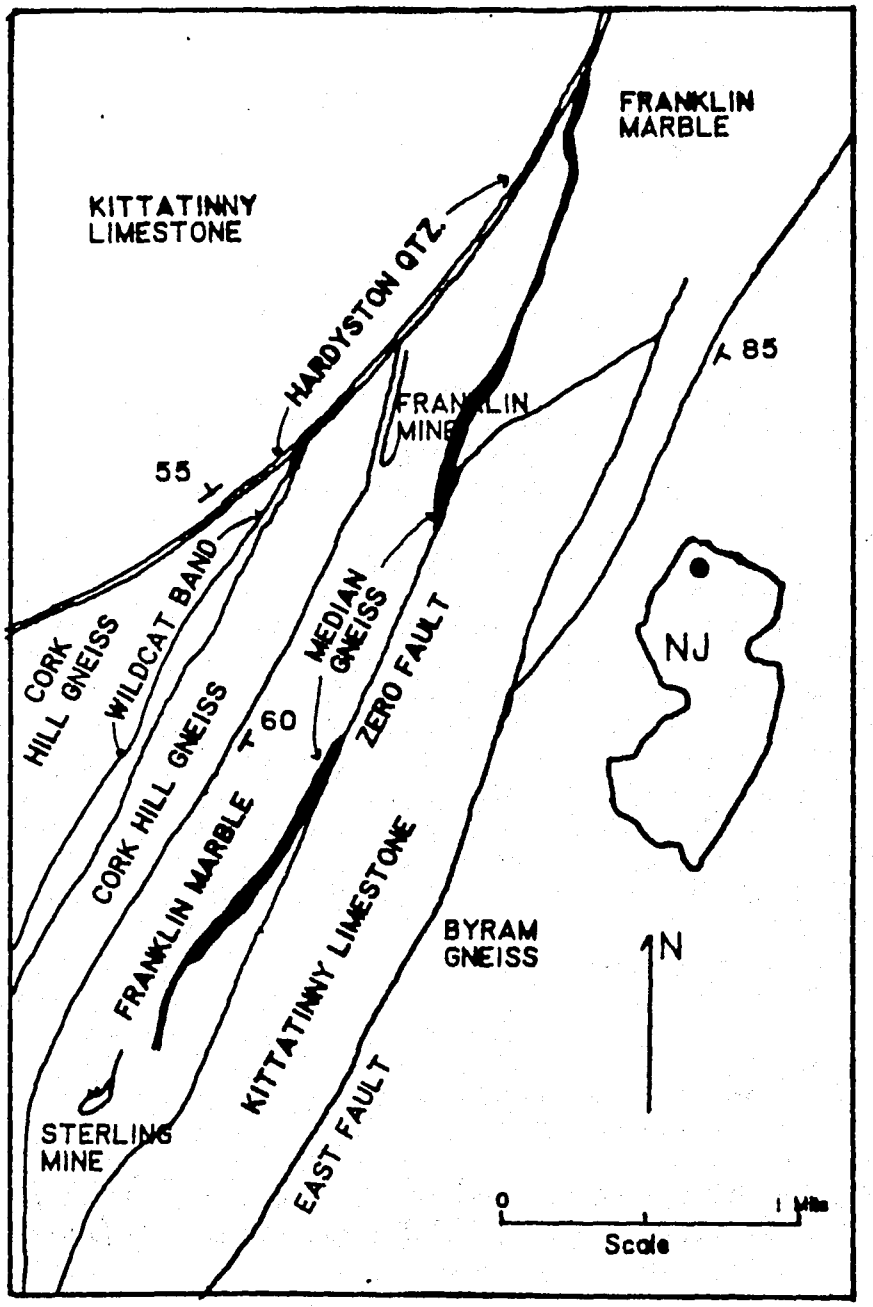

Figure 1. Sketch map of the Franklin-Sterling Hill area. From Frondel and Baum, 1974.

regionally metamorphosed to sillimanite-zone rank during the late Precambrian (Frondel, et al., 1974). These bodies were apparently exhumed during the late Precambrian as evidenced by an erosional surface which is uncomformably overlain by the Hardyston formation of early Cambrian age. Remnants of an oxidized zone on this erosional surface contained limonite, hemimorphite and other secondary minerals (Frondel, et al., 1974).

The Hardyston formation, which is predominately quartzite, is the basal formation of the region. It consists of metamorphic sandstone and quartz-pebble conglomerate which locally grade into sandy dolomite. Detrital franklinite is present locally in the quartzite. The Hardyston is comformably overlain by the Cambro-Ordovician Kittatiny formation which is dominantly dolomite and subordinately shaly or sandy dolomite with a few beds of limestone near the top (Hague, et al., 1956). The local stratigraphic column is given in Table 1.

The area has been affected by faulting and minor folding in the late Paleozoic as well as by intrusion of basic dikes probably during late Silurian time (Frondel, et al., 1974). Small granitic and pegmatitic dikes of late Precambrian age are present in the Franklin marble and associated gneisses (Frondel, et al., 1974). These pegmatic intrusions apparently

Table 1. Stratigraphic Column of the Franklin-Sterling Hill Area

Age	Formation	Remarks	Thickness
Cambro-Ordovician	Kittatinny	Mostly dolomitic limestone, in part shaly or sandy	760-910 m
Lower Cambrian	Hardyston	Conglomerate and quartzite	10 m
Precambrian	Pochuck Gneiss Series	Interlayered hornblende gneiss, microcline gneiss, locally with garnet or graphite, also local quartzite	Over 610 m
	Wildcat Marble	Coarsely crystalline marble	910 m
	Cork Hill Gneiss	Similar to Pochuck Series	240-310 m
	Franklin Marble	Coarsely crystalline marble, locally dolomitic	340-460 m
	Median Gneiss	Chiefly biotite gneiss	20-90 m
	Franklin Marble	As above	Unknown, over 150 m
	Hamburg Mountain Gneiss	Similar to Pochuck Series, intruded by Byram hornblende granite	710 m

NOTE: Table taken from Frondel and Baum (1974).

overprinted the Franklin deposit and were responsible for the formation of the extremely large variety of minerals present at this locality.

K-Ar and 40Ar-39Ar incremental-release ages were determined to be 768±15 to 819±18 my (average 790 my) and 869±20 to 949±24 my (average 900 my) on biotite and hornblende, respectively, from the Grenville basement gneiss of the northeastern Reading Prong (Dallmeyer, et al., 1975). These ages, as well as U-Pb zircon ages of the gneiss (1,060 my) in the New Jersey and New York Highlands indicate age dates for post-Grenville metamorphic cooling. These ages are in accord with dates deduced for the deposits from the overlying stratigraphy (Table 1) and place tighter constraints on the time and duration of metamorphism. Age differences should represent varying degrees of argon retention in the minerals dated. Hornblende retains argon below about 525°C whereas biotite retains argon below about 325°C. These ages suggest that cooling of the Grenville rocks from about 760°C (Carvalho, 1978) to 325°C took approximately 270 my (Fig. 2). This is a cooling rate of 1.6°C per million years.

General Structure and Mineralogy

The Sterling Hill ore body is a structurally complex isoclinal syncline with a long east limb and a shorter west

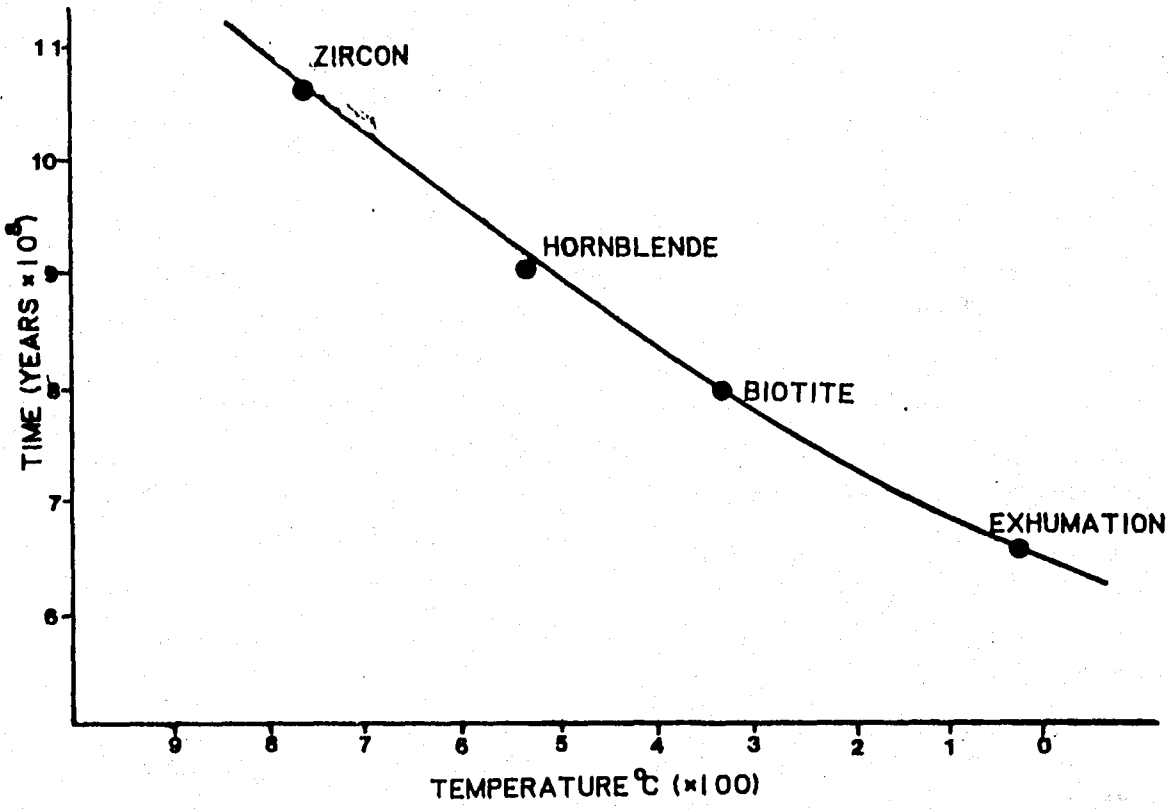

Figure 2. Pre-Cambrian cooling curve for Greenville sequence. From Carvalho, 1978.

Figure 2. Pre-Cambrian cooling curve for Greenville sequence. From Carvalho, 1978.

limb both of which dip 55° eastward (Fig. 3). Both the east and west limbs are joined by a cross-member which is greatly thickened in the middle portion. Near the middle of the west limb, the cross-member branches off and runs nearly parallel to the west limb and then doubles back and forms an intermediate synclinal fold, the eastern leg of which eventually joins the east limb. The end of the two limbs, the keel of the syncline, the thickened part of the cross-member and the latter junctions with the two limbs, plunge roughly parallel at 45°N 70°E (Metsger, et al., 1958).

The ore body consists of a series of complex attenuated isoclinal folds with the ore and the wall rock of the ore even more complexly folded than the surrounding country rock. This is exemplified by severely contorted bands of ore, boudin structure, and infolded wall rock, all of which indicate extreme plastic deformation. Metsger, et al. (1969) suggests that the complex folds may have developed as a result of downward movement of the deposit during metamorphism because of the relatively high density of the ore body compared with the surrounding Franklin marble.

The deposits occur in the Franklin marble which is coarse crystalline white marble generally well banded containing phlogopite, corundum, diopside, minor tourmaline, spinel, and sphene (Frondel and Baum, 1974). Graphite is ubiquitous in

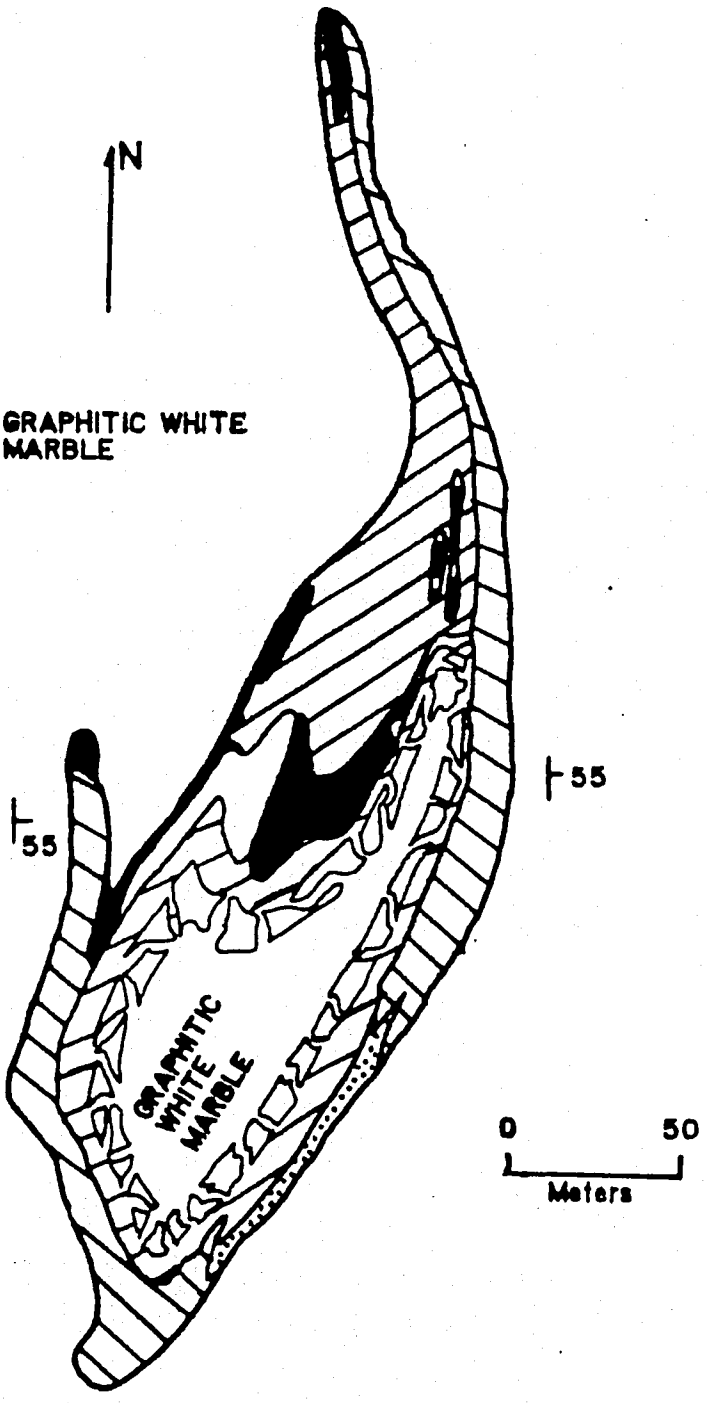

Figure 3. Geologic map of the Sterling Hill ore body, from Metsger, et al. (1958). See following page for legend.

ZONES

zincite band

Outer Zincite - flesh to red willemite and tephroite, zincite, non-magnetic franklinite, limestone.

Central Zincite - similar to outer zone, but with magnetic franklinite in eastern part.

Black Willemite - black willemite and tephroite, magnetic franklinite.

Gneiss - pyroxene, feldspar, biotite, hornblende.

Pyroxene - limestone, green and brown pyroxene, magnetic franklinite, biotite, garnet.

Franklinite - limestone and magnetic franklinite.

Brown Willemite - brown to dark brown willemite and tephroite, magnetic franklinite, limestone.

the marble except in and near the ore. A marble zone five feet thick which envelopes the ore body is graphite free, but otherwise is apparently identical with the country rock. Locally large masses of the marble have been dolomitized. This dolomitization appears to be related to joints, faults, and breccia zones (Metsger, et al., 1958).

The primary ore minerals are franklinite $[(Zn,Mn,Fe^{+2})(Mn,Fe^{+3})_2O_4]$, willemite (Zn_2SiO_4), and zincite (ZnO) which are disseminated in fluorescent manganoan calcite. According to Hague, et al. (1956), the estimated average composition of the ore mined at Sterling Hill is 33% franklinite, 16% willemite, and 1% zincite. These estimates are not necessarily representative of the mineral distribution of the deposit as a whole because the ore is selectively mined.

Description of Sample Locations

All samples collected for this study were obtained in June of 1981 and in January of 1982. Additional samples, which were collected by Carvalho (1978) in November of 1977, were also used in this study. The criterion used for sampling was to collect rocks which contained magnetic spinels. These magnetic spinels would either be magnetite, magnetic franklinite, or intergrowths of magnetite and franklinite, all

of which are indistinguishable with the unaided eye. Particular attention was payed to samples containing macroscopic gahnite because the two samples of magnetite-franklinite exsolution intergrowths that were found by Carvalho (1978) are enclosed in single crystals of green gahnite.

All samples were collected at the 500', 600', and 700-foot levels in the mine with the exception of the diamond drill-core samples. The core samples collected and prepared for study were selected by placing each core on its side and holding a strong magnet adjacent to it. Any sign of movement of the core indicated the presence of a magnetic phase and hence the possibility of magnetite-franklinite intergrowths.

Sample Series No. 5, which was collected by Carvalho (1978) was located on the 500-foot level approximately 10 feet east along the cross cut from the west limb. The rock at this location is white marble which contains diopside, minor franklinite, biotite and garnet. Discrete gahnite crystals up to 5 cm in length are common in the marble at this location.

500-Foot Level

1 South end of the 560 north stope on the west limb, 1240 feet west on the hanging wall. This rock contains magnetic spinels, calcite.

2-3-4 Entrance to old powder magazine, south side. Sample 2 contains non-magnetic franklinite, calcite, minor willemite and garnet. Number 3 contains magnetic spinels, calcite and minor willemite. Sample 4 contains slightly magnetic gahnite up to 4 cm, magnetic spinels, calcite and minor willemite.

5 560 north stope, 2 feet above footwall. The ore here contains non-magnetic franklinite, gahnite, and mangoan calcite.

600-Foot Level

14 Foot wall of the 1250 north stope. Contains magnetic spinel, willemite, and manganoan calcite.

15 North side of the 1180 north pillar, 10 feet above 600-foot level. This sample contains magnetic spinels, willemite and calcite.

16 Located 25 feet east of sample 15. Consists of magnetic spinels, willemite and manganoan calcite.

17 Footwall of the 1200-foot stope in the franklinite band. The rock contains magnetic spinels, willemite and manganoan calcite.

18 1160 north stope along strike of the franklinite band. Magnetic spinels and manganoan calcite.

19-20 1020 north stope at cross-cut. Both samples contain magnetic spinels, willemite and calcite.

21-22 Footwall drift of 1250 north stope. Sample 21 contains gahnite, biotite, rhodinite (?), tephroite (?) and manganoan calcite. Sample 22 contains magnetic spinels, minor mica, willemite, and manganoan calcite.

23 Branch of 1220 north cross-cut, 3 feet above Nason fault on the hanging wall. Magnetic spinels, trace willemite and manganoan calcite are present.

700-Foot Level

6 1120 north cross-cut on the hanging wall of the 1140-foot stope. This sample consists of two parts: part 1 contains magnetic spinels in a manganoan calcite matrix with minor willemint; part 2 contains non-magnetic franklinite in a non-fluorescent calcite matrix with minor willemite.

7 Footwall drift of 935 north stope. Contains massive, very slightly magnetic gahnite, biotite and minor calcite.

Diamond-Drill Hole Cores

8 No. 438 at 54 feet. Contains magnetic spinels with inclusions of willemite and calcite.

9 No. 432 at 71 feet. Core consists of magnetic spinels, calcite and willemite.

10 No. 441 at 32 feet. Massive gahnite, magnetic spinels with calcite and trace willemite.

11-12 No. 442 at 18.5 feet and 36.5 feet, respectively. Both contain magnetic spinels and calcite.

13 No. 432 at 100 feet. Consists of magnetic spinels and calcite.

OXIDES OF THE MAGNETITE-FRANKLINITE SERIES AT STERLING HILL

Spinel Structure

The spinel group of minerals, Fd3m, is face-centered cubic and its structure consists of 32 oxygen ions per unit cell which form a nearly cubic close-packed framework whose direction of close packing is the cubic diagonal [111]. There are 64 tetrahedral, or A sites and 32 octahedral, or B sites per unit cell. Only one-eighth of the A sites (8) and one-half of the B sites (16) are filled with cations so that the unit cell contains eight formula weights AB_2O_4. The sites occupied by cations are special sites in the sense that they lie at the intersection of symmetry elements. These sites, although mutually exclusive, are identical in that a translation of their origin by ½, ½, ½ will bring one set into coincidence with the other.

The large size of oxygen (.14μm) allows cations in the range of .05 m - .08 m to substitute in the A and B sites. If

the A sites are filled with divalent cations and the B sites are filled with trivalent cations the structure is referred to as a normal 2-3 spinel. An example of this is franklinite $[(Zn^{+2})(Fe^{+3})_2O_4]$. In some spinel the A site contains trivalent cations whereas the B sites contain both divalent and trivalent cations which gives rise to what is designated the inverse structure. Magnetite is an example of an inverse spinel, $[(Fe^{+3})(Fe^{+2}Fe^{+3})_2O_4]$. In both cases there is a net positive charge of 64 which is balanced by the 32 O^{-2} anions. It is also possible to have normal and inverse 2-4 spinels. Furthermore, it is important to point out that most spinels are neither fully normal nor fully inverse and have varying degrees of inverse or normal character.

The spinel structure has a large range of chemical composition and extensive solid solubility is common, especially at high temperatures. At least 30 different elements with valences ranging from +1 to +6 can proxy as cations in oxide spinels. This extensive substitution of cations in the oxygen framework is a result of the oxygen parameter, conventionally called μ. If the oxygen parameter equaled $\frac{1}{4}$ then the oxygen arrangement would give rise to a rigorous cubic-close-packing. However, μ does deviate from this value of $\frac{1}{4}$, but this deviation is so slight that the oxygen can be considered to be closed-packed. An increase in

μ corresponds to an enlargement of the tetrahedral coordination polyhedra and a compensating diminution in the octahedra (Lindsley, 1976) (Fig. 4). The unit cell can therefore expand or contract to accommodate cations of larger or smaller effective radii. It is this flexibility of the oxygen framework which gives rise to a large number of cations which can proxy in oxide spinels.

Ilmenite Structure

The rhombohedral series consists of several types of structures (Lindsley, 1976). One type is the ilmenite structure, $R\bar{3}$, which is a subgroup of the hematite structure, $R\bar{3}c$. The lower space group symmetry of the ilmenite-type structure is due to multiple types of cations in the structure which gives rise to ordering. Minerals with the ilmenite structure include ilmenite ($FeTiO_3$), pyrophanite ($MnTiO_3$), and geikielite ($MgTiO_3$).

Oxygen forms planes lying parallel to (0001) of the hexagonal cell [(111) of the rhombohedral cell] that are nearly but not quite hexagonal close packed. Within each plane are triplets of touching oxygens which are slightly separated so that the average oxygen-oxygen distance between triplets is greater than that for close packing (Fig. 5). These oxygen triplets in adjacent planes do not lie above one

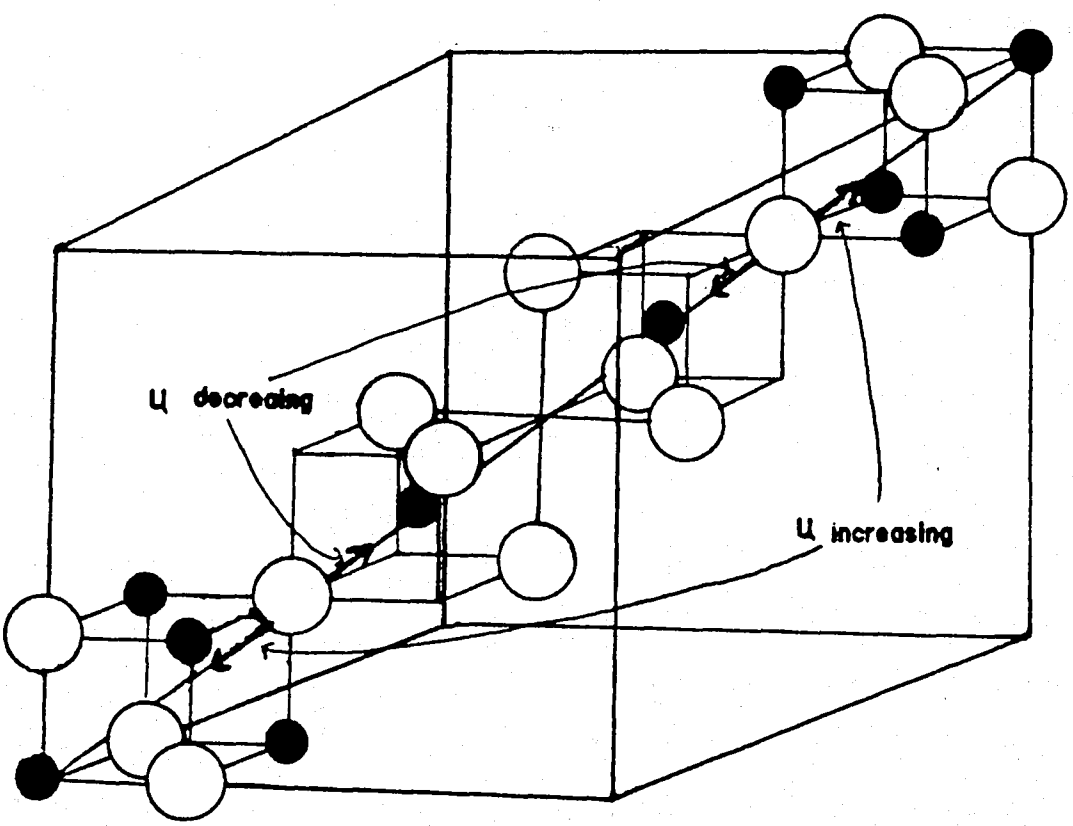

Figure 4. Details along a body diagonal of the spinel unit cell illustrating how changes in the oxygen parameter, μ, change with the relative sizes of the tetrahedral and octahedral sites.

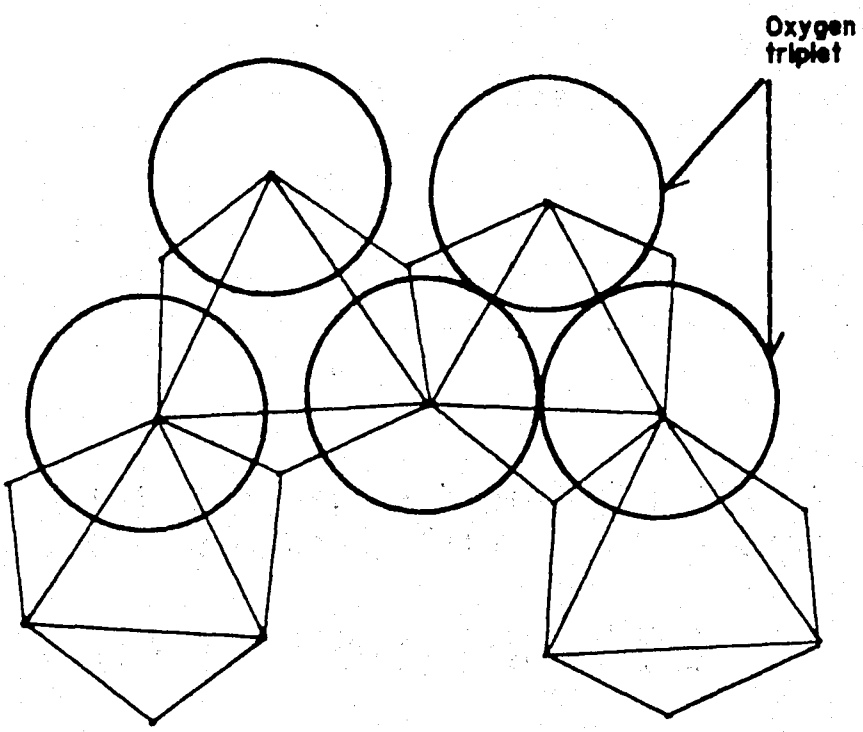

Figure 5. The ilmenite structure viewed down the hexagonal c axis illustrating the oxygen triplet and the coordination octahedra of oxygens.

another, but are offset so that above and below each triplet are three non-touching oxygens. An ideally hexagonal close packed oxygen framework consists of 18 octahedral interstitial sites per 18 oxygens. In the ilmenite structure, two-thirds of these sites are occupied by cations. It should be noted that these six-fold oxygen coordination polyhedra, although referred to as octahedra, are not true octahedra because of the distortion. The two opposite faces of these octahedra lie in the (0001) planes, which are the planes of the oxygen layers. For each octahedra, one of these faces is shared and one is unshared. The three oxygens comprising the shared face are the triplets and are essentially close packed whereas those in the unshared face lie slightly farther apart. The cations will lie somewhat closer to the planes of the unshared face than of the shared face, because they fall down between the separated oxygens. This is a result of electrostatic repulsion between the cations on either side of planes midway between the oxygen layers, rather than on those planes as they would for ideal hexagonal close packing.

The ilmenite structure is made up of Fe-O_3-Ti units, triplets of close packed oxygen with Fe on one side and Ti on the other. The sequence of cations along any [0001] axis is ...Fe-Ti-□-Ti-Fe-□-Fe..., where the hyphen represents intervening planes of oxygen layers. Every third potential

octahedral site is empty and the nearest cations to an empty site along [0001] are always two Fe or two Ti. The $Fe\text{-}O_3\text{-}Ti$ units are so arranged in (0001) that oxygen layers alternate with metal layers which themselves alternate between layers of Fe and layers of Ti.

Magnetite-Franklinite Exsolution Intergrowths

At high temperatures there is complete miscibility along the magnetite ($FeFe_2O_4$)-franklinite ($ZnFe_2O_4$) join. The occurrence of magnetite-franklinite exsolution intergrowths at the Sterling Hill zinc deposit suggests that at lower temperatures there is a miscibility gap in the solid-solution series whereby the originally homogeneous spinel exsolves topotactically parallel to the cube face (100). Of all the samples collected in this study, none contain magnetite-franklinite intergrowths, however, gahnite-franklinite intergrowths of the types described by Carvalho (1978) occur in most samples.

Samples 5-1 and 5-2, which were collected and studied by Carvalho (1978), contain highly fractured, translucent pale to dark green gahnite crystals each approximately 5 cm in length. These single crystals of gahnite contain exsolution intergrowths of magnetite and franklinite up to 1 mm in size constituting up to 5% of the crystal by volume. There are

Figure 6. Photomicrograph of magnetite-franklinite exsolution intergrowth. Light phase is magnetite. Reflected polarized light, oil immersion. The length of the bar scale is 20 μm. From Carvalho, 1978.

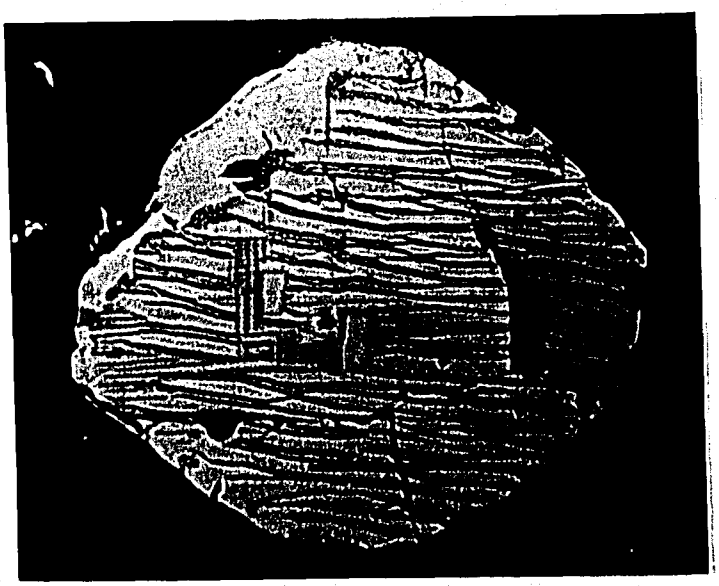

Figure 7. Photomicrograph of franklinite-magnetite exsolution intergrowth. Note the magnetite is the dominant phase. Reflected polarized light, oil immersion. The length of the bar scale is 20 μm. From Carvalho, 1978.

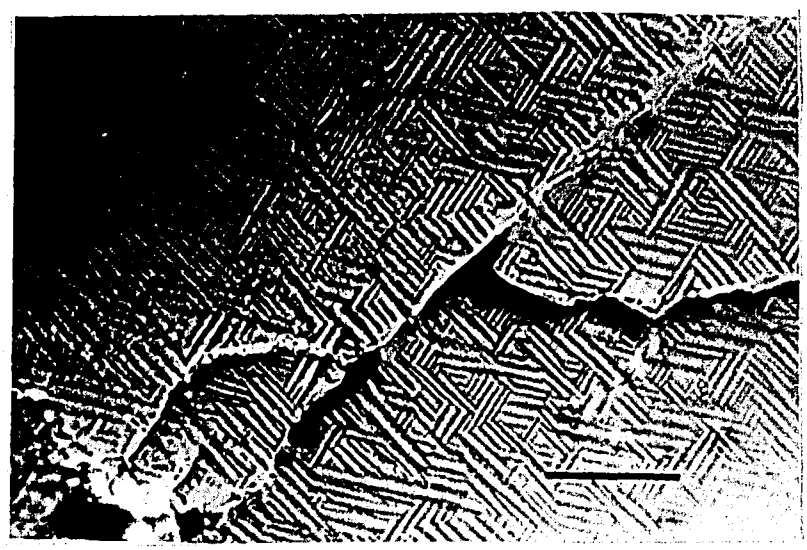

Figure 8. Photomicrograph of franklinite-magnetite exsolution intergrowth. Photomicrograph shows a Widmanstätten pattern with lamellae in three orientations. Plane of polished section is approximately normal to [111]. Reflected polarized light, oil immersion. The length of the bar scale is 15 μm. From Carvalho, 1978.

Figure 9. Photomicrograph of franklinite-magnetite exsolution intergrowth. Note the hematite (white phase) has selectively replaced the magnetite. Reflected polarized light, oil immersion. The length of the bar scale is 10 μm. From Carvalho, 1978.

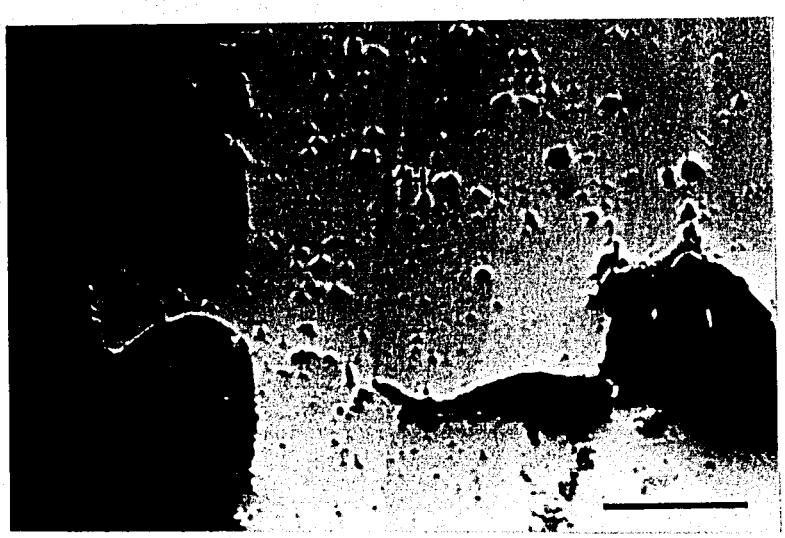

Figure 10. Photomicrograph of franklinite-magnetite exsolution intergrowth. Photomicrograph shows secondary zincite (Z) associated with twinned hematite (H). Reflected polarized light, oil immersion. The length of the bar scale is 10 μm. From Carvalho, 1978.

three variations of these exsolution textures which occur in the gahnite. First, where the intergrowths consist of two phases in about equal abundance, the magnetite occurs as two perpendicular sets of lamellae in the franklinite host (Fig. 6). The second type occurs when magnetite is the dominant phase, in this case the franklinite occurs as thin oriented lamellae in the magnetite host (Fig. 7). The third is a Widmanstätten-type intergrowth which shows two or three sets of lamellae depending on the orientation viewed (Fig. 8).

Locally, the magnetite-rich lamellae have been oxidized to hematite (Fig. 9) and in some cases the hematite replaced both the magnetite and franklinite (Fig. 10). The latter hematite commonly shows multiple twinning. Where the hematite has massively replaced the magnetite-franklinite intergrowths the hematite is found associated with anhedral zincite which probably formed by the reaction $ZnFe_2O_4 \rightarrow Fe_2O_3 + ZnO$. Some of the hematite which has selectively replaced magnetite appears to constitute a hematite-franklinite exsolution intergrowth. This is probably what Frondel and Klein (1965) observed when they reported the occurrence of hematite lamellae as exsolution bodies in franklinite.

Magnetite-Pyrophanite Exsolution Intergrowths

In addition to magnetite-franklinite exsolution intergrowths, sample 5-2 also contains magnetite-franklinite intergrowths in which the magnetite-rich lamellae contain an additional set of exsolution lamellae of another phase. This additional phase within the magnetite lamellae is distinctly anisotropic and occurs as three sets of lamellae (Fig. 11) all of which are oriented at high angles to the magnetite lamellae. These lamellae are, therefore, not oriented parallel to the common (100) plane of the magnetite-franklinite intergrowth, and appear to be oriented on (111) of the spinel host. Electron microprobe analysis as well as elemental X-ray maps and backscattered electron images of this phase indicate that the phase has a Mn/Ti atomic ratio approximately equal to one and contains neither Fe nor Zn. This phase, therefore, has the composition of pyrophanite ($MnTiO_3$) which possesses the ilmenite structure.

According to Ramdohr (1980), the occurrence of pyrophanite is similar to that of ilmenite which occurs commonly as the product of oxidation exsolution in many magnetite and franklinite ores and is less commonly found as a discrete mineral. It is known to occur in Cerro Iman, Uraguay, and Massamba, Mozambique (Ramdohr, 1980). Czamanske and Mihálik, 1972, report ilmenite-pyrophanite solid solutions

Figure 11. Photomicrograph of magnetite-franklinite exsolution intergrowth. Photomicrograph shows oriented exsolution lamellae of pyrophanite in the magnetite lamellae. Reflected polarized light, oil immersion. The length of the bar scale is 20 μm. From Carvalho, 1978.

as exsolution lamellae in magnetite of the Finnmarka igneous complex in Norway.

The common plane of exsolution is most likely (111) of the spinel and (0001) of the pyrophanite. Both these planes represent nearly close packed layers of oxygen so the interplanar spacing at the contact as well as the structure normal to the contact is similar. This gives rise to a low interfacial energy or a reduction in lattice strain at the grain boundary. This reduced strain yields a lower G (change in free energy) which would be necessary to nucleate and grow a second phase out of an originally homogeneous phase for a particular lattice orientation.

RESULTS OF ELECTRON AND X-RAY MICROANALYSIS

Magnetite, franklinite and pyrophanite intergrowths were analyzed for Fe, Zn, Mn, Ti, Al, and Mg with a JEOL 733 Superprobe equipped with secondary electron and backscattered electron detectors. Wavelength dispersive analysis of these elements were performed with an accelerating voltage of 15 KeV. Standards used were: 1) ilmenite from the Ilmen Mountains, USSR (U.S. Museum No. 96189) which contains 36.43 wt. % Fe, 27.40 wt. % Ti, and 3.87 wt. % Mn by wet chemical analysis, 2) a synthetic single crystal of ZnO, and 3) a

synthetic single crystal of $MgAl_2O_4$. All raw data were corrected for atomic number, absorption, and fluorescence effects. The resulting corrected analytical data were in terms of weight percent and atomic percent of the elements; oxygen values were computed by difference. An analysis of the magnetite-franklinite intergrowth which is devoid of the pyrophanite phase was reported by Carvalho (1978). Carvalho obtained the same elemental analysis with the exception of Mg using identical standards with an ARL electron microprobe with an accelerating voltage of 15 KeV.

Magnetite-Franklinite Exsolution Intergrowths

Sample 5-1 and 5-2 contain opaque bodies in gahnite which consist of regular oriented intergrowths of magnetite and franklinite. Electron microprobe analyses of these intergrowths from Carvalho (1978) are given in Table 2. Total iron is expressed arbitrarily as Fe_2O_3, zinc as ZnO, manganese as MnO, aluminum as Al_2O_3, and titanium as TiO_2. The calculated cation proportion based on one-hundred cations is also given in Table 2.

Carvalho used the following method to calculate the amount of ferrous and ferric iron present in the spinel. The weight percent of each metal was divided by the appropriate

Table 2. Electron Microprobe Analyses of Franklinite-Magnetite Intergrowths and Their Constituent Phases (from Carvalho, 1978)

	(1)	(2)	(3)	(4)	(5)	(6)	(7)
Fe_2O_3	66.0	98.6	100.2	81.0	88.9	81.5	87.5
ZnO	26.0	0.6	0.0	13.8	11.4	12.8	11.8
MnO	4.1	1.0	0.0	4.2	1.7	2.8	1.3
Al_2O_3	1.6	0.7	0.1	1.2	1.4	2.0	1.2
TiO_2	3.5	2.1	0.3	2.6	0.3	0.4	0.2
Total	101.2	103.0	100.6	102.8	103.7	103.1	102.0
			Atoms/100 Atoms				
Fe	65	95	100	78	85	81	85
Zn	25	1	0	13	11	12	11
Mn	5	1	0	5	2	3	1
Al	2	1	0	2	2	3	2
Ti	3	2	0	3	0	0	0
			Tetrahedral Sites/32 Oxygen				
Zn	6.0	0.1		3.1	2.5	3.1	2.7
Fe	1.1	7.4		3.6	4.7	3.8	4.8
Mn	1.1	0.3		1.1	0.5	0.8	0.4
Sum	8.2	7.8		7.8	7.7	7.7	7.8
			Octahedral Sites/32 Oxygen				
Al	0.6	0.3		0.4	0.5	0.8	0.4
Fe	14.6	15.2		15.0	15.4	15.1	15.5
Ti	0.8	0.5		0.6	0.1	0.1	0.1
Sum	16.0	16.0		16.0	16.0	16.0	16.0

Table 2 (cont.)

Molecular Percentages of End Members

$ZnFe_2O_4$	85	1	46	35	45	36
$FeFe_2O_4$	15	99	54	65	55	64

NOTE: Total Fe expressed as Fe_2O_3.

1. Franklinite Host, Sample 5-2; average of 2 analyses.
2. Magnetite Lamellae, Sample 5-2; average of 2 analyses.
3. Hematite replacing Magnetite-Franklinite Intergrowth.
4. Broad-Beam Analyses of Magnetite-Franklinite Intergrowth, Sample 5-2 (Area Scanned: 40 x 32 μm); average of 6 analyses.
5. Broad-Beam Analyses of Magnetite-Franklinite Intergrowth, Magnetite Lamellae Dominant, Sample 5-2 (Area Scanned: 40 x 32 μm).
6. Broad-Beam Analyses of Magnetite-Franklinite Intergrowth, Sample 5-1; average of 4 analyses (Area Scanned: 40 x 32 μm).
7. Broad-Beam Analyses of Magnetite-Franklinite Intergrowth, Magnetite Lamellae Dominant, Sample 5-1 (Area Scanned: 40 x 32 μm).

atomic weight to obtain the atomic proportions. The oxygen proportion was then calculated assuming all the iron is trivalent and the cation proportions were normalized to 32 oxygen ions. Zinc and manganese were assumed to be divalent and assigned to the tetrahedral sites. The remaining octahedral sites were filled with aluminum, titanium, and Fe^{+3} any residual iron was assumed to be Fe^{+2} and assigned to the tetrahedral sites. However, some of the Fe^{+3} in the octahedral sites are actually Fe^{+2} which would be needed to offset the high charge of the Ti^{+4}. Therefore, the tetrahedral sites contain Zn^{+2}, Mn^{+2}, and Fe^{+2}, and the octahedral sites contain Al^{+3}, Ti^{+4}, Fe^{+3}, and minor Fe^{+2}.

This method of calculation is in accord with the crystal-field stabilization energies of the cations involved. The octahedral site preference energy in Kcal/g - atomic weight, for Zn^{+2}, Mn^{+2}, Fe^{+3}, Fe^{+2}, Mg^{+2}, Al^{+2}, and Mn^{+3} are -31.6, -14.7, -13.3, -9.9, -5.0, -2.5, and 3.0, respectively (Muller and Roy, 1974). The larger the number, the greater the affinity of the cation for the octahedral site. The actual polyhedral location of Fe is also a function of the spinel structure, normal vs. inverse character of the spinel.

The iron and zinc content of the franklinite is in general agreement with the average composition of discrete grains of franklinite from Sterling Hill (66Fe, 23Zn, 11Mn per

100 cations) as reported by Frondel and Baum (1974). The magnetite lamellae (Table 2, Analysis 2) contains minor amounts of Zn, Mn, Al, and Ti (TiO_2=2%) by weight. An analysis of the hematite which partly replaced magnetite and franklinite showed that it contains minor amounts of Al and Ti (Table 2, Analysis 4).

Magnetite-Franklinite-Pyrophanite Intergrowths

Sample 5-1 consists of a magnetite-franklinite intergrowth in which the magnetite-rich lamellae contain a second set of exsolution lamellae. These lamellae are anisotropic and appear to be oriented on the (111) plane of the magnetite. These lamellae are as thick as 1μm and 10μm long. Because of its orientation on the (111) plane and its anisotropic character, it will henceforth be referred to as the rhombohedral phase. The minute dimensions of these lamellae causes problems with microanalysis. One problem is the difficulty of placing an electron-probe on the center of this phase and not partially on the surrounding magnetite matrix. A second problem is the effect of electron beam-specimen interactions because once the beam strikes the specimen, the electrons will spread out in a pear shape below the surface. This spreading will cause excitation in the surrounding magnetite matrix which will result in

contamination of the analysis. Because of these problems, backscattered electron images and elemental X-ray maps of the rhombohedral phase were obtained to complement electron microprobe analysis in order to optimize the data available.

Electron microprobe data for the rhombohedral phase are given in Table 3, and an analysis of the magnetite and franklinite lamellae of the intergrowth as well as area scans of the intergrowth are shown in Table 4. The values reported in Tables 3 and 4 are the cations normalized to one-hundred cations on an atomic basis. Mn/Ti and Fe/Zn ratios are shown for all analysis and Table 3 also contains Fe/Mn ratios from the rhombohedral phase analysis. Molecular percentages of the end members were also calculated for selected phases.

In addition to microprobe analysis, the three phases were also examined by looking at the atomic number contrast from backscattered electron images (Fig. 12). The higher the average atomic number in a phase, the brighter the phase appears. These images show that the franklinite is brighter than magnetite. This would be expected because of the concentration of Zn (Z=30) in franklinite as opposed to magnetite were the cations are dominantly Fe (Z=26). Within the magnetite is the rhombohedral phase which is darker than

Table 3. Electron Microprobe Analyses of Pyrophanite Lamellae in Magnetite$_{ss}$ of Magnetite-Franklinite Exsolution Intergrowths

	Cations/100 Cations								
	(1)	(2)	(3)	(4)	(5)	(6)	(7)	(8)	(9)
Mg	0.0	0.0	0.1	0.1	0.2	0.0	0.0	0.1	0.2
Al	0.0	0.0	4.5	2.4	1.5	0.0	0.6	0.0	0.1
Ti	20.6	9.9	22.9	33.4	22.0	41.7	28.3	18.6	35.9
Fe	54.2	74.1	30.1	24.4	49.3	10.4	40.3	60.8	18.2
Mn	23.6	13.5	35.3	38.6	25.7	46.7	29.7	19.0	44.6
Zn	1.6	1.8	1.0	1.2	1.6	1.3	1.3	1.5	1.1
	100.0	99.3	99.9	100.1	100.3	100.1	100.2	100.0	100.1
Mn/Ti	1.2	1.4	1.2	1.2	1.2	1.1	1.1	1.0	1.2
Fe/Mn	2.3	5.5	0.9	0.6	1.9	0.2	1.4	3.2	0.4
Fe/Zn	33.3	41.4	31.4	20.2	31.2	8.3	30.5	40.0	17.2
	Molecular % End Members of Magnetite Host								
$ZnFe_2O_4$	8	7	10	14	9	38	9	7	17
$FeFe_2O_4$	92	93	90	86	91	62	91	93	83

Average Mn/Ti = 1.16

Table 4. Electron Microprobe Results of Magnetite Solid-Solution, Franklinite Solid-Solution and Broad-Beam Analysis

	Cations/100 Cations					
	(1)	(2)	(3)	(4)	(5)	(6)
Mg	0.5	0.3	0.0	0.0	0.0	0.0
Al	0.9	2.2	2.1	2.3	1.6	2.0
Ti	0.5	3.0	2.8	3.2	4.0	3.3
Fe	88.6	62.7	67.2	64.0	71.2	67.5
Mn	2.0	5.0	4.5	4.8	5.7	5.0
Zn	8.0	28.3	23.6	25.8	17.6	22.3
	100.5	101.5	100.2	100.1	100.1	100.1
Mn/Ti	3.7	1.7	1.6	1.5	1.4	1.5
Fe/Zn	11.1	2.2	2.9	2.5	4.0	3.0
	Molecular % End Members					
$ZnFe_2O_4$	25	93	72	76	54	68
$FeFe_2O_4$	75	7	6	--	17	6
$MnFe_2O_4$	--	--	14	14	17	15
Fe_2TiO_4	--	--	9	9	12	10

1. Magnetite lamellae, average of 3 analyses.
2. Franklinite lamellae, average of 4 analyses.
3. Broad-beam analysis of magnetite-franklinite-pyrophanite intergrowths (Area Scanned: 25 x 30 μm).
4. Broad-beam analysis of magnetite-franklinite-pyrophanite intergrowths (Area Scanned: 25 x 30 μm).
5. Broad-beam analysis of magnetite-franklinite-pyrophanite intergrowths (Area Scanned: 25 x 30 μm).
6. Average of broad-beam analysis of 3, 4, and 5.

Table 4. Electron Microprobe Results of Magnetite Solid-Solution, Franklinite Solid-Solution and Broad-Beam Analysis

	Cations/100 Cations					
	(1)	(2)	(3)	(4)	(5)	(6)
Mg	0.5	0.3	0.0	0.0	0.0	0.0
Al	0.9	2.2	2.1	2.3	1.6	2.0
Ti	0.5	3.0	2.8	3.2	4.0	3.3
Fe	88.6	62.7	67.2	64.0	71.2	67.5
Mn	2.0	5.0	4.5	4.8	5.7	5.0
Zn	8.0	28.3	23.6	25.8	17.6	22.3
	100.5	101.5	100.2	100.1	100.1	100.1
Mn/Ti	3.7	1.7	1.6	1.5	1.4	1.5
Fe/Zn	11.1	2.2	2.9	2.5	4.0	3.0
	Molecular % End Members					
$ZnFe_2O_4$	25	93	72	76	54	68
$FeFe_2O_4$	75	7	6	--	17	6
$MnFe_2O_4$	--	--	14	14	17	15
Fe_2TiO_4	--	--	9	9	12	10

1. Magnetite lamellae, average of 3 analyses.
2. Franklinite lamellae, average of 4 analyses.
3. Broad-beam analysis of magnetite-franklinite-pyrophanite intergrowths (Area Scanned: 25 x 30 μm).
4. Broad-beam analysis of magnetite-franklinite-pyrophanite intergrowths (Area Scanned: 25 x 30 μm).
5. Broad-beam analysis of magnetite-franklinite-pyrophanite intergrowths (Area Scanned: 25 x 30 μm).
6. Average of broad-beam analysis of 3, 4, and 5.

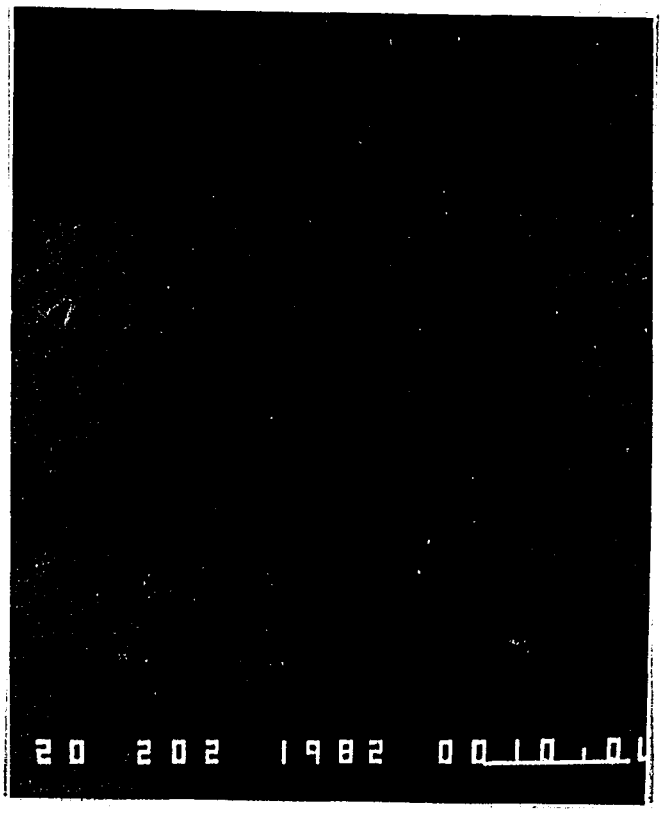

Figure 12. Backscattered electron image of magnetite-franklinite-pyrophanite exsolution intergrowths. Dark phase is pyrophanite, intermediate phase is magnetite, and light phase is franklinite. The length of the bar scale is 10 μm.

the magnetite indicating it possesses an average atomic number less than 26 (Fe).

Elemental X-ray mapping for Fe, Zn, Mn, Ti, Al and Mg was done for the three phases to ascertain the distribution of these elements in the intergrowths. Iron (Fig. 13) is concentrated primarily in the magnetite and secondarily in the franklinite, but it is virtually absent in the rhombohedral phase. Zinc (Fig. 14) is concentrated in the franklinite whereas both magnetite and pyrophanite contain only trace amounts of zinc. Manganese (Fig. 15) and titanium (Fig. 16) are clearly concentrated in the rhombohedral phase, but the franklinite contains only minor amounts of both of these elements and the magnetite contains almost none. Aluminum (Fig. 17) is present in only minor amounts, but it shows a preference for franklinite whereas magnesium (Fig. 18) is present in trace amounts and does not appear to be concentrated in any particular phase. The rhombohedral phase, therefore, consists exclusively of manganese and titanium. The atomic-number contrast from backscattered electrons is in accord with this assessment because the atomic number of Mn is 25 and Ti is 23, therefore the rhombohedral phase should and does appear darker than the magnetite.

Inasmuch as the rhombohedral phase contains only Mn and Ti, all other elements reported for this phase in Table 3 must

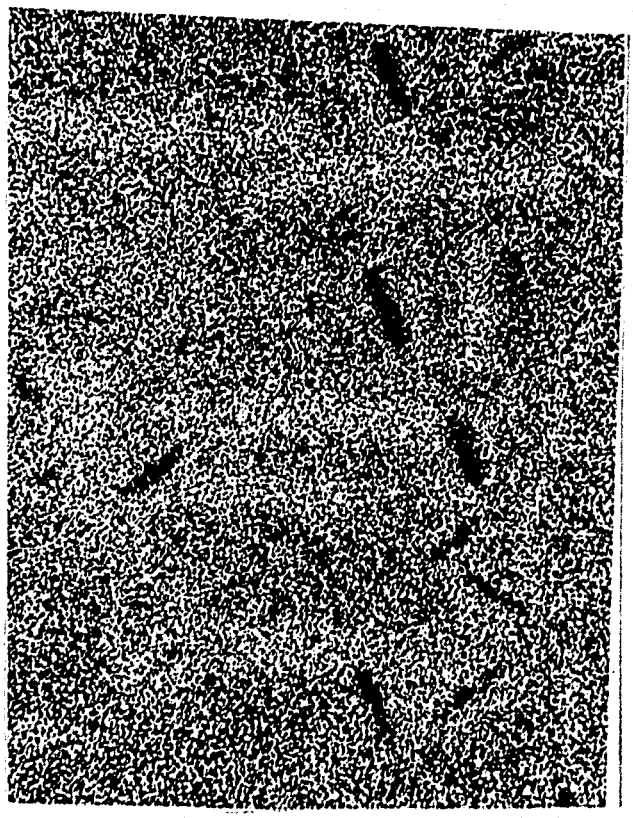

Figure 13. Iron X-ray map. Bright areas indicate presences of iron.

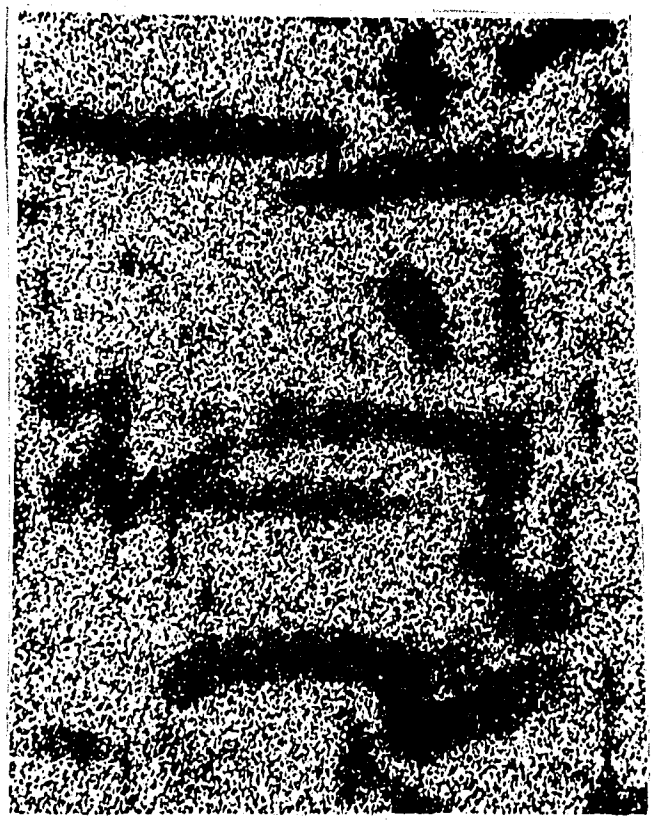

Figure 14. Zinc X-ray map. Bright areas indicate presences of zinc.

Figure 15. Manganese X-ray map. Bright areas indicate presences of manganese.

Figure 16. Titanium X-ray map. Bright areas indicate presences of titanium.

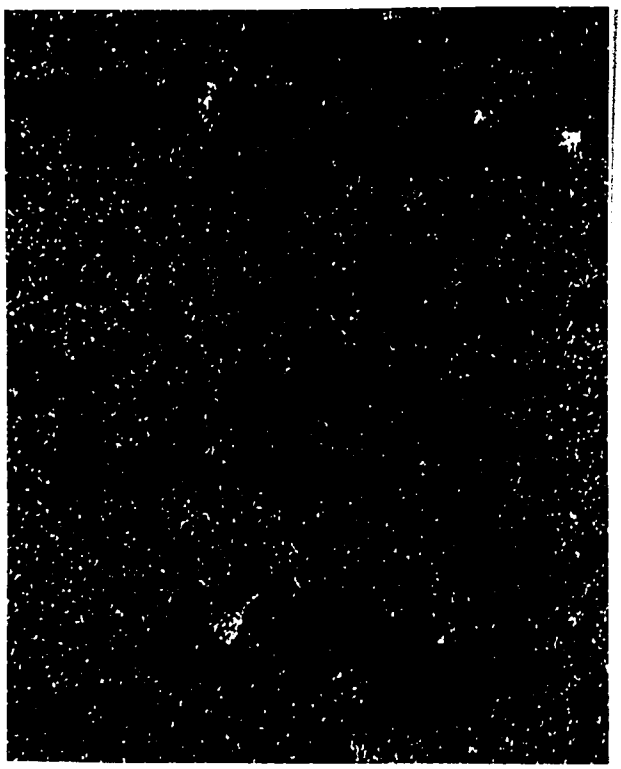

Figure 17. Aluminum X-ray map. Bright areas indicate presences of aluminum.

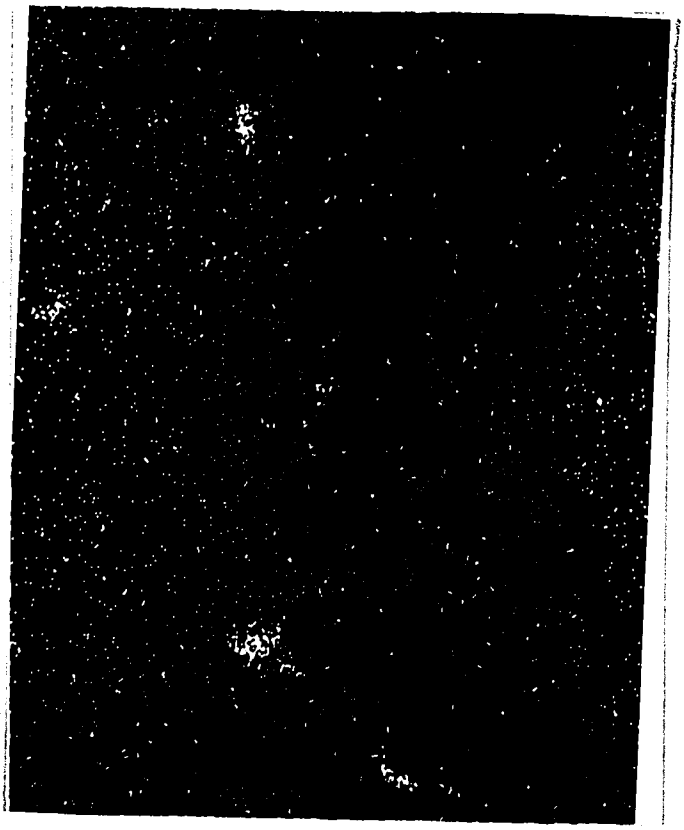

Figure 18. Magnesium X-ray map. Bright areas indicate presences of magnesium.

be the result of contamination from the surrounding magnetite. The relative amount of contamination can be determined from the Fe/Mn atomic ratio. The greater the deviation of this ratio from one, the greater the degree of contamination. Although the degree of magnetite contamination varies, it can be seen that the Mn/Ti ratio is essentially constant for the rhombohedral phase and averages to 1.16. Inasmuch as the magnetite host contains about 2.0% Mn and about 0.5% Ti with a Mn/Ti ratio of 3.7, only minor amounts of Mn and Ti can be included in the analysis of the rhombohedral phase from contamination from the magnetite. Analysis 2, Table 3 of the rhombohedral phase shows the highest Fe/Mn ratio, 5.5, and also yields the highest Mn/Ti ratio which is 1.4. The higher Mn/Ti ratio is undoubtedly due to some minor contamination from magnetite because the Mn/Ti ratio for magnetite is 3.7. It is considered that, although the average Mn/Ti ratio is 1.16, minor enhancement of the true ratio occurred due to minor contamination from the magnetite matrix which has a relatively high Mn/Ti ratio. Therefore, 1.16 must be a maximum Mn/Ti ratio and the true ratio is probably slightly less and closer to 1.0 in accord with the ideal formula of pyrophanite ($MnTiO_3$), which has the ilmenite structure. This stoichiometry as well as textural relations and optical

anisotropy indicates that this phase is pyrophanite which exsolved on the (111) plane of the host.

A photograph of all three phases was point-counted (350 points) to determine the relative volume percentages of the three phases in franklinite-magnetite-pyrophanite intergrowths. This point count showed that, by volume, franklinite comprises 40%, magnetite 43%, and pyrophanite 17%. The magnetite solid-solution before the second exsolution took place thus constituted approximately 60% by volume of the intergrowth. Table 5 shows the calculated original composition of this magnetite solid solution before the second unmixing took place. This calculation assumes that the pyrophanite consists of 28% by volume and magnetite consists of 72% by volume of the original magnetite exsolution lamellae and that density differences are negligible. This composition, which is an approximation, indicates that during the first exsolution event most of the Mn and Ti selectively partitioned into the magnetite-rich phase as opposed to the franklinite-rich phase.

EXPERIMENTAL WORK

Introduction

The major objective of this study was the experimental determination of the position and shape of the solvus loop in the ideal binary system magnetite ($FeFe_2O_4$)-franklinite

Table 5. Calculated Composition of Unexsolved Magnetite Solid-Solution in the Magnetite-Franklinite Intergrowths before Exsolution of Pyrophanite

	(1)	(2)	(3)	(4)	(5)
Mg	0.5	--	0.36	--	0.36
Al	0.9	--	0.65	--	0.65
Ti	0.5	50	0.36	14.0	14.36
Fe	88.6	--	63.79	--	63.79
Mn	2.0	50	1.44	14.0	15.44
Zn	8.0	--	5.76	--	5.76
	100.5	100.0	72.36	28.0	100.36

1. Magnetite solid-solution after pyrophanite exsolution; see analysis 1, Table 4.
2. Ideal pyrophanite composition ($MnTiO_3$).
3. 72% of magnetite solid-solution composition (see text for explanation).
4. 28% of ideal pyrophanite composition (see text for explanation).
5. Calculated composition of magnetite solid-solution before exsolution of pyrophanite.

($ZnFe_2O_4$). The mode of attack was to synthesize first a series of homogeneous spinels representing both pure end members and intermediate compositions on the join $FeFe_2O_4$-$ZnFe_2O_4$ in a high temperature gas-mixing furnace under controlled fO_2. Lattice parameters of these homogeneous spinels were determined by X-ray powder diffractometry and a Vegard plot of lattice parameter (a_o) vs. composition was constructed. Some of the homogeneous single-phase spinel products and selected mechanical mixtures of two different spinel products were then reacted hydrothermally at selected temperature intervals and constant pressure all under controlled fO_2 in order to equilibrate these spinels at lower temperatures and thus determine the solvus in the temperature range selected. Products of the hydrothermal runs were characterized by X-ray powder diffractometry and the results were integrated with the newly constructed Vegard plot.

Synthesis of Homogeneous Spinels

Homogeneous spinels were synthesized in 10% molar intervals along the $FeFe_2O_4$-$ZnFe_2O_4$ join using the appropriate stoichiometric proportions of SPEX high-purity oxides (Fe_2O_3 5-9's, and ZnO 6-9's). The oxides for each composition were mixed and ground in a sintered alumina mortar and pestal under acetone for fifteen minutes and then pelletized.

Inasmuch as the iron in this system has multiple oxidation states, with the exception of the iron in the zinc ferrite (franklinite) end member (which is ideally all ferric), it was necessary to control the fO_2 during the syntheses in order to control the valence state of the iron in the spinel. The fO_2 was controlled by gaseous buffering techniques described in detail by Ulmer (1971) and use of a high-temperature gas mixing furnace.

About 0.3 grams of each pelletized oxide mixture was placed in a ceramic boat which in turn was placed in a silica tube. The silica tube was then inserted through a horizontal cylindrical alumina tube in the gas-mixing furnace and connected to the plastic tubing of the gas-mixing circuit.

The fO_2 for pure magnetite was controlled by mixing reagent grade CO_2 and H_2 in appropriate proportions as determined by Dienes, et al. (1974). Intermediate compositions were synthesized under flowing CO_2 whereas the $ZnFe_2O_4$ end member was synthesized in air. All spinels were synthesized at 1200°C for four hours with the exception of $FeFe_2O_4$ which was synthesized at 1150°C (Table 6). At the end of the run, the CO_2 or CO_2-H_2 gas mixture was cut off and the system was flushed with argon gas for about five minutes. Subsequently, the furnace was moved aside on a track and the samples were thus rapidly quenched. The argon gas in the

Table 6. Conditions for Synthesis of Homogeneous Spinels on the Join Magnetite ($FeFe_2O_4$) - Franklinite ($ZnFe_2O_4$)

Bulk Composition	Temp., °C	-log fO_2*	Total time, hours
$FeFe_2O_4$ (Magnetite)	1150	4.0	4
$(Fe_{.9}Zn_{.1})Fe_2O_4$	1200	3.95	4
$(Fe_{.8}Zn_{.2})Fe_2O_4$	1200	3.95	4
$(Fe_{.7}Zn_{.3})Fe_2O_4$	1200	3.95	4
$(Fe_{.6}Zn_{.4})Fe_2O_4$	1200	3.95	4
$(Fe_{.5}Zn_{.5})Fe_2O_4$	1200	3.95	4
$(Fe_{.4}Zn_{.6})Fe_2O_4$	1200	3.95	4
$(Fe_{.3}Zn_{.7})Fe_2O_4$	1200	3.95	4
$(Fe_{.2}Zn_{.8})Fe_2O_4$	1200	3.95	4
$(Fe_{.1}Zn_{.9})Fe_2O_4$	1200	3.95	4
$ZnFe_2O_4$ (Franklinite)	1200	air	4

*All spinels were synthesized under flowing CO_2 with the exception of 1) $FeFe_2O_4$ which was synthesized in an atmosphere consisting of a mixture of $H_2 + CO_2$, and 2) $ZnFe_2O_4$ which was synthesized in air.

system kept the sample in an inert environment during the quench; otherwise the sample would have been exposed to more oxidizing conditions and possible re-equilibration since valence stability fields are both fO_2 and temperature dependent. The product of each run was accessed by X-ray powder diffractometry to determine if the oxide reaction went to completion and if all observed diffraction maxima correspond to the spinel structure.

Determination of Spinel Composition by Lattice Parameter Measurement

Each synthesized homogeneous spinel was analyzed by X-ray powder diffractometry using Cu-K_α radiation in conjunction with a Philips APD-3600 automated powder diffractometer. All samples were scanned at a rate of 1°2θ/minute with scans ranging from 30°-80°2θ using an internal standard of silicon powder (5-9's purity) to correct for peak positions. All 2θ values in this range were converted to d-values by using values of .15406, .15418, and .15444 nm for Cu-K_{α_1}, Cu-K_α, and Cu-K_{α_2}, respectively. These d-values, along with their corresponding hkl's, were entered into the cell-edge refinement program of Appleman and Evans (1973) which produced the unit-cell edge, a_o, through a least-squares fit of these data (Table 7).

The data in Table 7 have been integrated with those of Stead (1980) and both sets of data are shown graphically in a Vegard plot of lattice parameter (a_o) vs. composition (Fig. 19). A least-squares linear regression of these data from both this study and that of Stead (1980) was done to determine how well these data approach that of a straight-line plot. The correlation coefficient, r, for a_o vs. composition for these data is -.983. The straight-line equation for these data is $a_o = -.0005X + 8.4484$ where X is the mole percent magnetite. This equation was used to determine the composition of the spinel phase(s) in the products of the hydrothermal runs described below.

Hydrothermal Experiments

Introduction

There are several experimental methods which may be employed to determine the equilibrium phase relations in a system which may contain a miscibility gap. These methods, which control time, temperature, fO_2, and, in some cases, pressure, include: 1) dry exsolution experiments in which an attempt is made to exsolve either high-temperature synthetic spinels of intermediate composition or natural homogeneous spinels of intermediate composition; 2) homogenization

Table 7. Lattice Parameters for Various Compositions Along the Magnetite ($FeFe_2O_4$) - Franklinite ($ZnFe_2O_4$) Join

Composition	Lattice Parameter (Å)
Mag_{100}	8.393
Mag_{90}	8.397
Mag_{90}	8.399
Mag_{80}	8.411
Mag_{70}	8.415
Mag_{60}	8.420
Mag_{50}	8.422
Mag_{50}	8.425
Mag_{40}	8.431
Mag_{30}	8.437
Mag_{20}	8.438
Mag_{10}	8.444
Mag_{10}	8.439
Mag_{0}	8.446

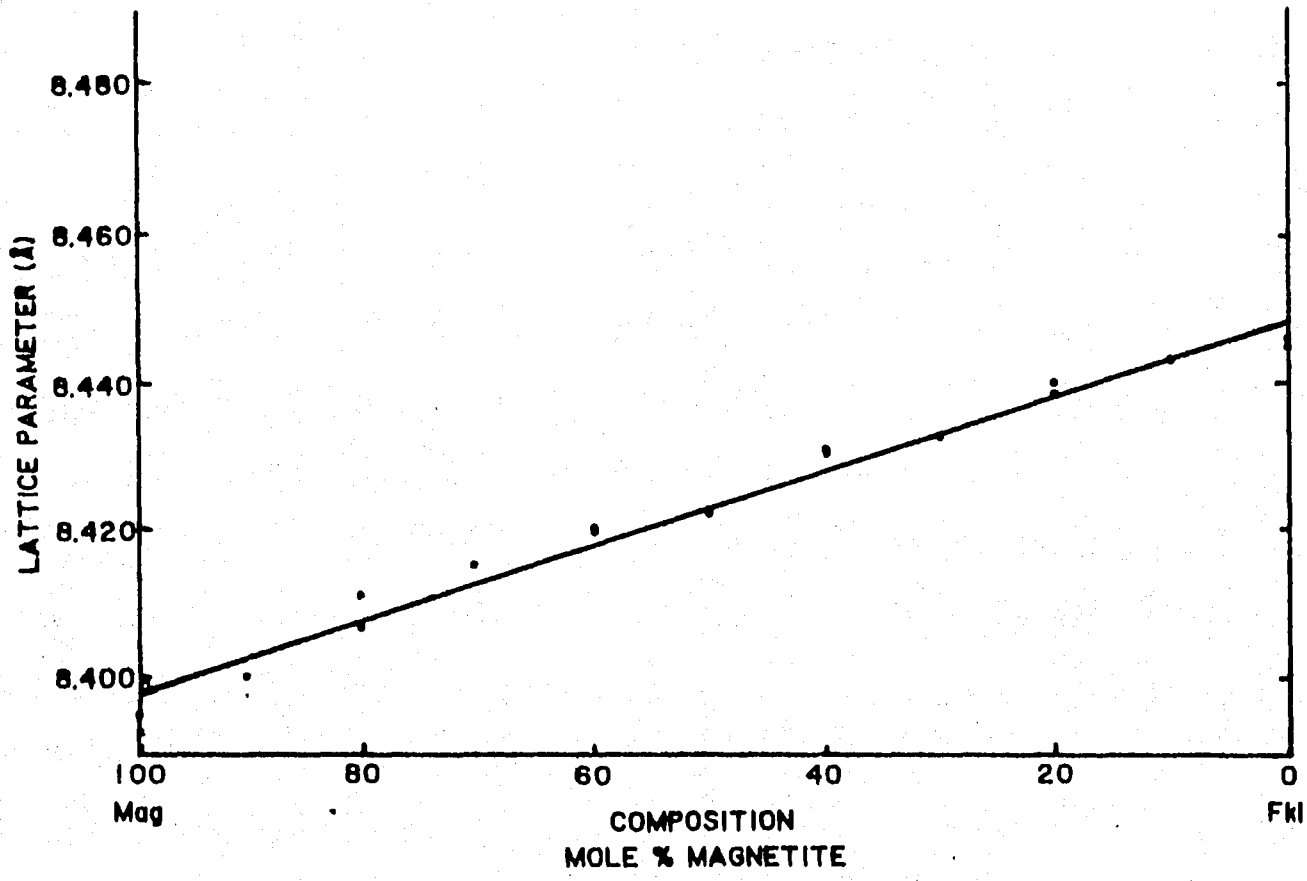

Figure 19. Vegard plot of lattice parameter versus composition along the magnetite ($FeFe_2O_4$) - franklinite ($ZnFe_2O_4$) join.

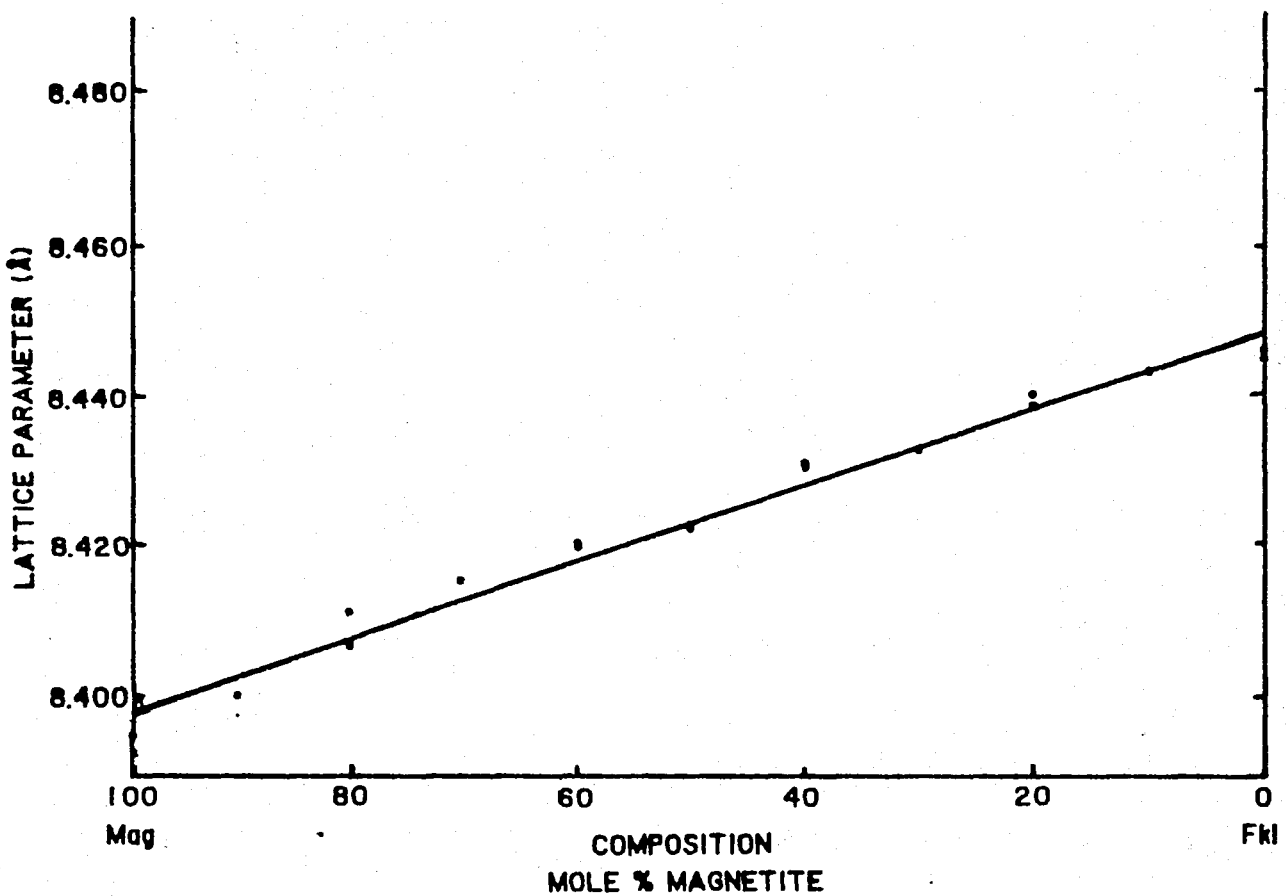

Figure 19. Vegard plot of lattice parameter versus composition along the magnetite ($FeFe_2O_4$) - franklinite ($ZnFe_2O_4$) join.

experiments, in which naturally exsolved material is homogenized into a single phase; and 3) hydrothermal experiments, in which a supercritical fluid such as H_2O is used to promote growth and nucleation of crystals, and enhance the rate of approach to equilibrium. Of the three methods mentioned, the most favorable and the one used in this study is (3), hydrothermal experimentation. Its advantages are; 1) enhancement of kinetics, 2) the use of high-purity synthetic spinels which results in more accurate phase relations because chemical contamination of a system may yield false boundaries within a stability field, and 3) the ability to verify the results on the same type of material by reversed reactions, that is, where phase or assemblage A is converted to B and then B is converted back to A under identical physical conditions.

Control of Oxygen Fugacity

In the system $FeFe_2O_4$-$ZnFe_2O_4$, iron is both divalent and trivalent except for pure $ZnFe_2O_4$, in which the iron is ideally only ferric. Thus, it was necessary to choose a buffering technique in which both valence states of iron could be maintained during the run. This problem was solved by using solid-solid buffering techniques. The buffer used was the lining on the bomb wall which consists of René No. 41

metal, a nickel-bearing iron alloy. When the hydrothermal bomb is new, reducing conditions prevail in the bore but, during use, an oxide coating develops and the oxygen fugacity of the bomb wall approaches that of the nickel-nickel oxide buffer. The NNO buffer lies in the magnetite stability field (Fig. 20) which makes it an ideal choice because both divalent and trivalent iron can coexist.

The charge was sealed in Pt or $Ag_{80}Pd_{20}$ capsules with H_2O. At relatively high temperatures and pressures, the water inside the capsule will dissociate by the reaction $2H_2O \rightarrow 2H_2+O_2$. Pt and $Ag_{80}Pd_{20}$ behave as a semipermeable membrane which allows protons (hydrogen ions) to diffuse back and forth so that the hydrogen fugacity in the region of the buffer surrounding the capsule is imposed on the internal system (Eugster and Wones, 1962). Once fH_2 equilibrium is attained, the system can be considered closed to all components. The fH_2 controls fO_2 which in turn controls the valence state of the iron so that in the case of the nickel-nickel oxide solid-solid buffer iron is both divalent and trivalent.

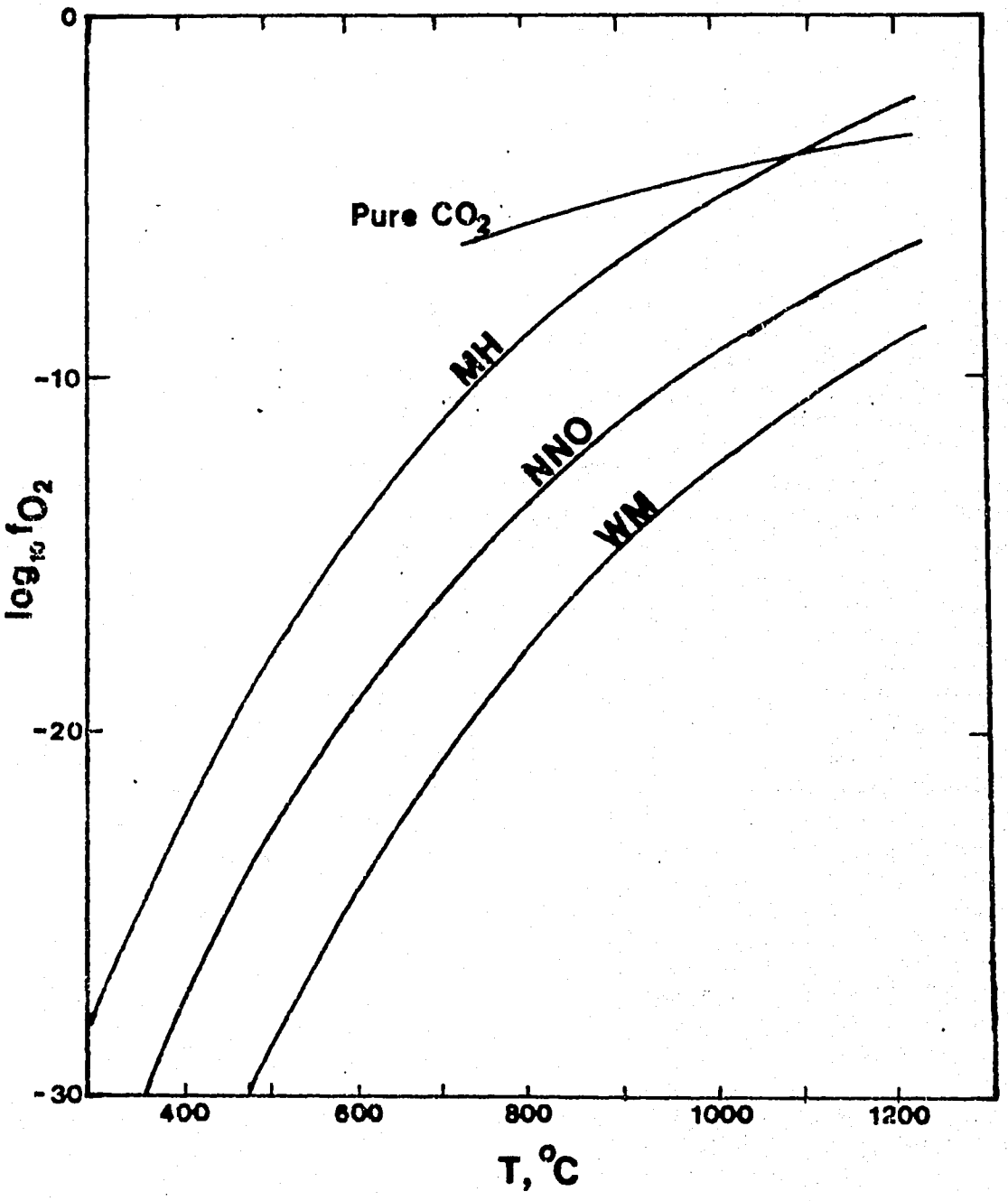

Figure 20. Oxygen fugacities as functions of temperature for selected solid-solid buffers and pure CO_2 at 1 atmosphere. Pressure effects are very small for solid-solid buffers. MH - magnetite-hematite; NNO - nickel-nickel oxide; WM - wüstite-magnetite. (Modified from Lindsley, 1976.)

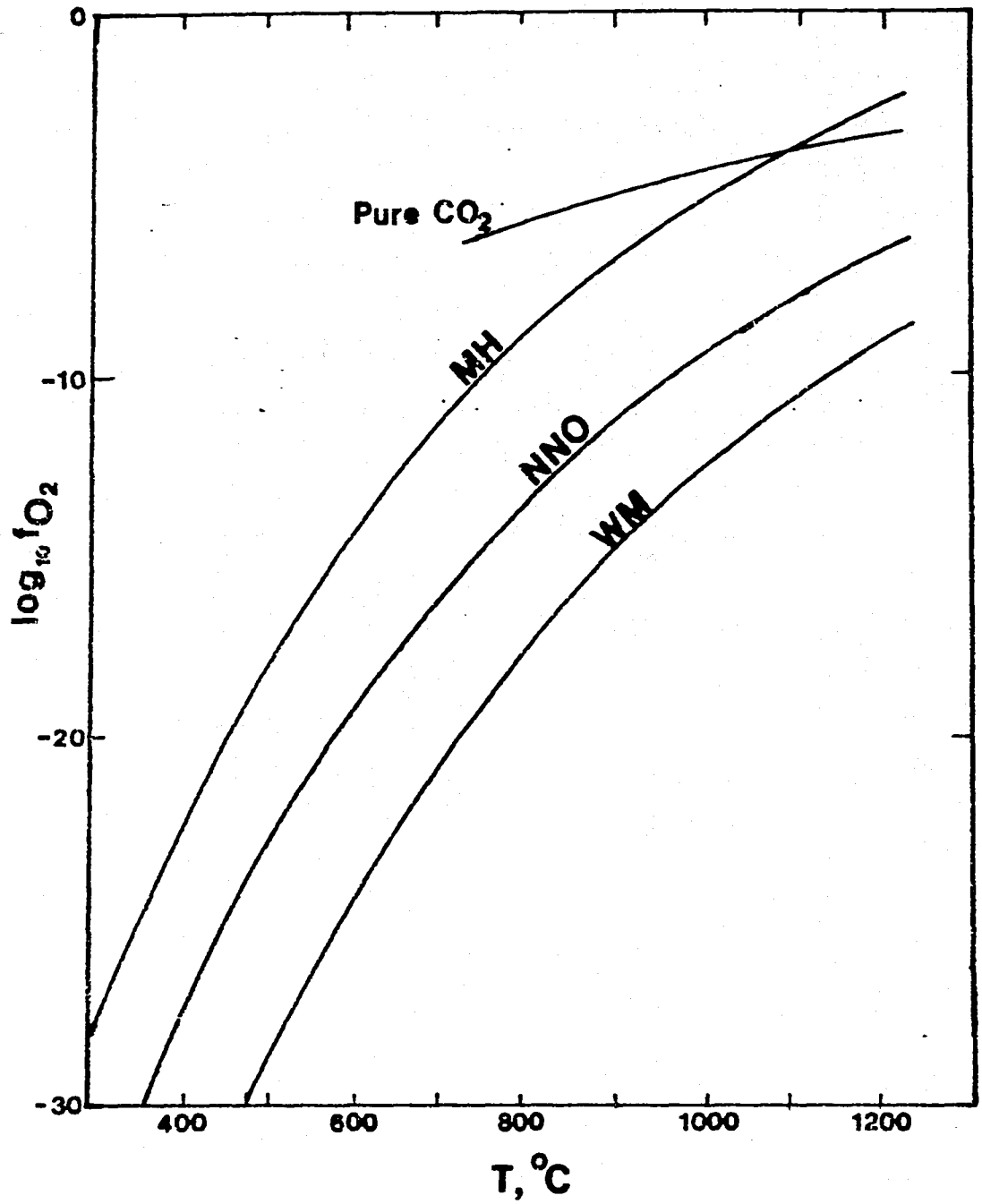

Figure 20. Oxygen fugacities as functions of temperature for selected solid-solid buffers and pure CO_2 at 1 atmosphere. Pressure effects are very small for solid-solid buffers. MH - magnetite-hematite; NNO - nickel-nickel oxide; WM - wüstite-magnetite. (Modified from Lindsley, 1976.)

Methods and Techniques

In order to accurately assess the degree of approach to equilibrium, all experiments were reversed so that two types of samples were reacted hydrothermally at each temperature selected. Starting materials were homogeneous spinels which, as previously mentioned (see section on Synthesis of Homogeneous Spinels), were synthesized from high-purity oxides under flowing CO_2 at 1200°C. The reactants for the first type of experiments were homogeneous spinels with a composition of Mag_{50}. The second type was a mechanical equimolar mixture of two homogeneous spinels of compositions Mag_{90} and Mag_{10}, respectively, with a bulk composition of Mag_{51}. Ideally, the attainment of equilibrium would be indicated by identical products from both sets of experiments.

The mechanical equimolar mixture was prepared by grinding equal weights of Mag_{90} and Mag_{10} in a sintered alumina automatic mortar and pestal for about one hour. This helped promote a more uniform distribution, intimate contact of particles, and reduction of particle size. The homogeneous spinel was not ground as fine because particle size should not affect exsolution significantly.

It is essential with respect to kinetics to have a minimal grain size or maximum surface area to volume ratio for the mechanical mixture because the reaction mechanism is

essentially a grain-boundary diffusionary process. There is a tradeoff with grinding to minute particle sizes to promote kinetics because the grinding process breaks down the long range order, at least on a scale detectable with X-ray diffraction. However, during the run there is a sintering effect whereby the grains will grow and the degree of crystallinity is enhanced as a function of both time and temperature. At low temperatures the sintering effect is minimal and chemical equilibrium may be attained long before the crystals have grown enough to restore an acceptable long-range order with respect to the X-ray diffraction. If this condition is suspected, the samples must be allowed to react longer than the time needed to achieve chemical equilibrium.

Pt and $Ag_{80}Pd_{20}$ metal tubing with a internal diameter of 3 mm, outside diameter of 3.6 mm, and a wall thickness of 0.3 mm were used for hydrothermal experiments with capsule lengths ranging between 13-16 mm. These metals were chosen because: 1) noble metals do not react with the sample, although Pt has a tendency to absorb and alloy with iron at high temperatures, and 2) the lattice of these metals is such that protons can diffuse back and forth through the wall so that these capsules act as semipermeables membrane which is essential in controlling fO_2.

Each capsule was crimped at one end with a needle-nosed pliers and sealed with either a carbon-arc welder or an oxygen-acetylene microtorch. The appropriate amount of deionized water was then placed in the bottom of the capsule with a calibrated syringe. The amount of water placed in each capsule varied (between 3 and 11 µl H_2O) because of the differential expansion of water as a function of temperature (Kennedy and Holser, 1966) (Table 8). Approximately 80 to 100 milligrams of charge was then placed in the capsule on top of the water. In this manner, with the water under the charge, there is minimal chance of vaporization of the fluid during the weld. The open end was then cleaned thoroughly to help insure a good weld, crimped shut, the second crimp being parallel to the first, and finally welded. During the final weld, the capsule was partially submerged in water which served as a heat sink to prevent evaporation of water during welding.

All welds were thoroughly checked by; 1) visual inspection under the binocular microscope, 2) ultrasonically vibrating the capsule to see if the charge seeped out, and 3) subjected to a hot-plate test. In the hot-plate test, the capsules were weighed, then placed on a hot plate at about 150°C for ten minutes, allowed to cool and reweighed. A

weight loss greater than about 0.0001 grams would indicate that water vapor escaped through an opening in the capsule.

Once the welds were checked and found to be satisfactory, the capsules were flattened slightly longitudinaly and parallel to the direction of both crimps. This is done so that when the capsule collapses from the external water pressure during the run, the strain will be uniform and the probability of rupture will be decreased. The capsules containing the homogeneous spinels and the mechanical mixture were then placed in the bottom of a cold-seal cone-seat hydrothermal pressure vessel with a ¼-inch bore. A stainless-steel filler rod was placed in the bore of the bomb to minimize convection of the hydrothermal fluid and decrease the thermal gradient. The bomb was the partially filled with deionized water and sealed.

Hydrothermal experiments were carried out at 0.1 GPa in the temperature range of 400°C-900°C at 50° temperature intervals. Run times ranged from 5 to 104 days (see Table 8). The furnaces were controlled within ±3°C. At the end of each run, the hydrothermal bombs were rapidly removed from the oven and quenched with compressed air.

Products of the hydrothermal runs were characterized by X-ray powder diffractometry. The difference in the lattice parameter of franklinite and magnetite is small, about 0.05Å

Table 8. Conditions of Hydrothermal Experiments in the System $FeFe_2O_4$ and $ZnFe_2O_4$ at 1 Kbar

Experimental Reactants				
Single-Phase Homogeneous Spinel	Mixture of Two Homogeneous Spinels*	Temp., °C	Duration, Days	Water in Capsule, µl.
Mag_{50}		900	5	3
	Mag_{51}	900	5	3
Mag_{50}		850	11	4
	Mag_{51}	850	11	4
Mag_{50}		800	16	5
	Mag_{51}	800	16	5
Mag_{50}		750	68	7
	Mag_{51}	750	68	7
Mag_{50}		700	75 ± 10	8
	Mag_{51}	700	75 ± 10	8
Mag_{50}		650	50	9
	Mag_{51}	650	50	9
Mag_{50}		600	50	9
	Mag_{51}	600	50	9
Mag_{50}		550	104	10
	Mag_{51}	550	104	10
Mag_{50}		500	61	11
	Mag_{51}	500	61	11
Mag_{50}		450	50	11
	Mag_{51}	450	50	11
Mag_{50}		400	68	11
	Mag_{51}	400	68	11

*Two-phase reactants consist of a mechanical mixture of Mag_{10} and Mag_{90}.

so that in order to detect peak splitting, it was necessary to use an X-ray tube with an anode with a fairly low atomic number and to scan in the back-reflection region to attain maximum resolution for possible peak splitting. The products were therefore scanned with Fe-Kα radiation at a scan rate of 1/8°2θ/min with particular reference to the configuration of the peaks resulting from the (642) and (731) diffraction maxima of the spinel structure. The products were also scanned with Cu-Kα radiation using a Philips APD-3600 automated powder diffractometer at 1/3°2θ/min to measure accurately the position of the peaks by using the 'second derivative peak algorithm program' developed by the Philips Company. The position of the peaks was corrected by using an internal standard of high-purity silicon. The positions of the (642), (731), and (800) diffraction maxima of the spinel structure were used to determine the unit-cell edge, (a_o) of the spinel phases (Table 9). By substituting a_o in the equation $a_o = -.0005X + 8.4484$, the composition of each spinel phase was determined through use of the unit-cell edge - composition diagram for the system $FeFe_2O_4$-$ZnFe_2O_4$ (Fig. 19).

Table 9. Results of Hydrothermal Experiments in the System $FeFe_2O_4$ - $ZnFe_2O_4$

Run*	Lattice Parameter (Å)	Products
900H	8.424	Mag_{49}
900M	8.417	Mag_{63} - minor Zn_2SiO_4
850H	8.422	Mag_{53}
850M	8.418	Mag_{61} - minor Zn_2SiO_4
800H	8.420	Mag_{57}
800M	8.414	Mag_{69} - minor Zn_2SiO_4
750H	8.424	Mag_{48}
750M	8.423	Mag_{51}
700H	8.420	Mag_{56}
700M	8.418	Mag_{61} - minor Zn_2SiO_4
650H	8.418	Mag_{61}
650M	8.406	Mag_{85}
600H	8.422	Mag_{53}
600M	8.414	Mag_{68}
550H	8.422	Mag_{53}
550M	8.411	Mag_{75}
500H	8.424	Mag_{48}
500M	8.419	Mag_{59}
450H	8.425	Mag_{46}
450M	8.437 - 8.410	$Mag_{23\pm6}$ - $Mag_{77\pm10}$
400H	8.425	Mag_{46}
400M	8.434 - 8.411	Mag_{29} - Mag_{74}

*Number indicates temperature of Run (°C), H - reactant was homogeneous spinel, M - reactant was mechanical mixture of Mag_{10} and Mag_{90}.

Results

The products of the hydrothermal runs are given in Table 9. The results of these runs are summarized as follows:

1. Minor willemite (Zn_2SiO_4) was found in the products of most of the mechanical-mixture reactants in the temperature range 700-900°C. This is due to minor silica contamination derived from the agate mortar used in crushing the hard sintered pellets of the homogeneous spinels used for the mechanical mixtures.

2. Zinc, especially in the mechanical mixture of spinels, appears to have selectively dissolved in the aqueous phase in the hydrothermal runs, thus resulting in a shift in the composition of the new homogeneous spinel phase toward a more magnetite-rich composition.

3. All of the original homogeneous spinel reactants (Mag_{50}) remained single-phase in the temperature interval explored (400°C-900°C).

4. All mechanical mixtures of spinel reactants at or above 500°C appear to have homogenized to a single spinel phase, although most of these single-phase products show a composition shift toward magnetite.

5. The runs at 400°C and 450°C show a partial approach to equilibrium in the time frame of these experiments.

6. The product of the mechanical mixture for runs at 400°, 450°, and 500°C are poorly crystalline as shown by broad X-ray diffraction peaks because of the lack of long range order, with respect to X-ray diffraction in the short run (or sintering) times.

DISCUSSION

The primary objective of this study was to determine experimentally the solvus in the ideal binary system $FeFe_2O_4$-$ZnFe_2O_4$ and to relate these phase relations with naturally occurring magnetite-franklinite exsolution intergrowths to determine a minimum peak temperature of regional metamorphism at the Sterling Hill zinc deposit. Experimental results from this study indicate that the

consolute temperature of the miscibility gap lies below 500°C. This, in turn, indicates that unmixing of magnetite-franklinite solid solution occurred below this temperature. The bulk composition of the original homogeneous single-phase spinels corresponding to the natural exsolution intergrowths is $Mag_{55}Fkl_{45}$, and, for those in which the magnetite lamallae are dominant, the bulk composition is $Mag_{65}Fkl_{35}$ (Table 2). Since these originally homogeneous spinels have intermediate compositions and assuming a nearly symmetrical solvus these intergrowths most likely exsolved near the consolute temperature of the hypothetical miscibility gap which may be at or below 400°C based on the observation that the 400°C run of the homogeneous spinels showed no sign of unmixing after 68 days (Table 8). Further investigation of the subsolidus phase relations below 500°C is not recommended because the solvus is too low to be useful as a geothermometer and experimental run times to achieve equilibrium may take as long as a year.

One of the magnetite-franklinite exsolution intergrowths in sample 5-2 contains pyrophanite exsolution lamellae within the magnetite-rich lamellae. Analysis 6, Table 4 shows that the original homogeneous spinel was highly enriched in Mn and Ti. As a result of this complex chemistry, the Mn-Ti-rich magnetite-franklinite solid solution also exsolved into a

magnetite-rich phase and a franklinite-rich phase. The calculated composition of this magnetite-rich phase (Table 5) indicates that during exsolution the Mn and Ti selectively partitioned into the magnetite-rich solid solution. The franklinite-rich phase has essentially the same composition as exsolved franklinite in the Mn-Ti-poor intergrowths of samples 5-1 and 5-2 (see analysis 2, Table 4 and analysis 1, Table 2). As the temperature decreased further, the Mn and Ti-rich magnetite lamellae exsolved pyrophanite ($MnTiO_3$). Pyrophanite is a mineral which rarely occurs as a discrete independent mineral. However, it occurs quite similarily to ilmenite as a product of oxidation exsolution in magnetite and franklinite ores (Ramdohr, 1980). It is found as exsolution intergrowths in magnetite in Cerro Iman, Uraguay, and Massamba, Mozambique (Ramdohr, 1980), also at the Finnmarka igneous complex in Norway (Czamanske and Mihålik, 1972), as well as other localities.

Crystallochemical consideration by Czamanske and Mihålik, (1972) and Haggerty (1976), on the preferred distribution of Mn^{+2} and Mn^{+3} between cubic and rhombohedral phases may explain the occurrence of pyrophanite in the magnetite-rich lamellae. The ionic radii for octahedral coordination are; Fe^{+2} = 0.86Å, Fe^{+3} = 0.73Å, Mn^{+2} = 0.91Å, Mn^{+3} = 0.58Å and Ti^{+4} = 0.69Å whereas in tetrahedral coordination Fe^{+3} = 0.57Å,

Mn^{+2} = .75Å, and Mn^{+3} = 0.57Å (Whittaker and Muntus, 1970). Ti will occupy the octahedral sites in Ti-rich magnetites. The inverse spinel structure of the magnetite as well as site preference energies will cause about half of the Fe^{+3} to be tetrahedrally coordinated. Fe^{+2} will occupy the octahedral sites as opposed to Mn^{+2} because Fe^{+2} has a greater affinity for the octahedral site and its size, 0.86Å, is closer to Ti (0.69Å) than Mn^{+2} (0.91Å). The Mn in the magnetite as well as the pyrophanite is thought to be mainly divalent because of the low temperatures which must have prevailed as evidenced by the experimental work done in this study and the low oxygen fugacity due to the buffering effect of the magnetite. This Mn must dominantly occupy the tetrahedral sites in the magnetite structure and the appreciable mismatch between Fe^{+3} (0.57Å) and Mn^{+2} (0.75Å) will make the spinel unstable at low temperatures thus resulting in unmixing.

Electron microprobe analysis indicates a Mn to Ti atomic ratio of approximately one for the exsolved phase. This composition in the spinel structure forces all Ti to be octahedral and thus the tetrahedral sites would be filled with Mn^{+2}. The remaining Mn^{+2} and any Mn^{+3} would go into the octahedral sites. A spinel structure of this composition would be highly unlikely to develop because of the large size differences between Ti^{+4} (0.69Å) and Mn^{+2} (0.91Å) in the

octahedral sites would make the structure highly unstable. The ilmenite structure would decidedly be favored under these conditions because, in this structure, all catons are in octahedral coordination and in accord with symmetry constraints the layers of cations consist of either all Ti or all Mn.

If this idea is correct, then fO_2 clearly had a major bearing on the conditions of exsolution, that is, with respect to retaining the Mn as Mn^{+2}. This type of exsolution may be somewhat analogous to ilmenite-magnetite 'oxidation exsolution' described by Buddington and Lindsley (1964). Buddington and Lindsley discuss the idea that although ilmenite commonly develops on the (111) plane of magnetite this is not true exsolution but oxidation 'exsolution'. True exsolution of titanomagnetite solid solution would produce an ulvospinel-rich phase exsolving in the (100) planes of a magnetite host. For this reaction to take place, unusually reducing conditions must prevail during cooling to permit ulvospinel to nucleate and grow along the magnetite-ulvospinel solvus. Under more normal conditions, ilmenite develops because of the following reasons. A small range of ilmenohematite solid solution close to $FeTiO_3$ in composition can coexist with a wide range of titanomagnetite solid solution at intermediate to low temperatures (Lindsley, 1976).

The compositions of the coexisting spinel and rhombohedral phases plotted as a function of temperature and fO_2 show that the slope of most contours are steeper than the buffer curves. This means that upon cooling, either along a buffer curve or in the presence of constant composition, a given titanomagnetite solid solution will be oxidized. The result will be a high-Ti ilmenohematite solid solution exsolving from a host of titanomagnetite. The resulting magnetite will become more enriched in the magnetite component. The textures of this exsolution will show ilmenite platelets parallel to the (111) planes of magnetite.

The temperature-composition-oxygen fugacity relations for the system Mn_3O_4-Mn_2TiO_4-$MnTiO_3$-Mn_2O_3 may yield similar conditions of solution and exsolution to its Fe analogue. If this is so, the pyrophanite may be a result of 'oxidation exsolution' and not true exsolution.

CONCLUSIONS

Experimental results of this study show that the consolute temperature of the solvus in the magnetite ($FeFe_2O_4$)-franklinite ($ZnFe_2O_4$) binary system is below 500°C, and that the solvus is too low for use as a geothermometer.

In accord with these experimental results, the naturally occurring magnetite-franklinite exsolution intergrowths must have formed below 500°C. Because the originally homogeneous magnetite-franklinite solid solution contained appreciable amounts of Mn and Ti two unmixing events occurred. The first unmixing event, which most likely took place below 500°C, resulted in a franklinite-rich phase with a chemistry almost identical to franklinite lamellae in magnetite in unmixed spinels in which little Mn or Ti was present; and a Mn-Ti-rich magnetite. Upon further cooling a second unmixing event took place in the Mn-Ti-rich magnetite resulting in the development of the rhombohedral phase pyrophanite ($MnTiO_3$) parallel to the (111) planes of the magnetite host.

The originally homogeneous Mn-Ti-rich magnetite-franklinite solid solution occurs only a few millimeters away from the Mn-Ti-poor magnetite-franklinite solid-solution which did not exsolve pyrophanite. This difference in composition of the original spinel phases is in accord with Squiller's (1976) and Squiller and Sclar's (1980) idea that chemical equilibrium at Sterling Hill took place on a scale of only a few millimeters resulting in good intragranular homogeneity and poor intergranular homogeneity.

The occurrence of pyrophanite at either the Sterling Hill or Franklin ore bodies was not known before this study. This occurrence of pyrophanite, therefore, constitutes the 287th mineral found in the Franklin-Sterling district.

REFERENCES

Appleman, D. E. and Evans, H. T., Jr., 1973, JOB 9214: Indexing and least squares refinement of powder diffraction data: U.S. Geological Survey, Computer Contrib. 20, 67p.

Buddington, A. F. and Lindsley, D. H., 1964, Iron-titanium oxide minerals and synthetic equivalents: Journal of Petrology, V. 5, p. 310-357.

Carvalho, A. V., III, 1978, Gahnite-franklinite intergrowths at the Sterling Hill zinc deposit, Sussex County, New Jersey: an analytical and experimental study: Lehigh University, M.S. thesis, 231p.

Czamanske, G. K. and Mihálik, P., 1972, Oxidation during magmatic differentiation, Finnmarka Complex, Oslo Area, Norway: Part I, the opaque oxides: Journal of Petrology, V. 13, p. 493-509.

Dallmeyer, et al., 1975, Incremental $^{40}Ar/^{39}Ar$ ages of biotite and hornblende for the NE Reading Prong: their bearing on late Proterozoic thermal and tectonic history: G.S.A. Bull., V. 86, p. 1435-1443.

Deines, P., Nafziger, R. H., Ulmer, G. C., and Woermann, E., 1974, Temperature-oxygen fugacity tables for selected gas mixtures in the system C-H-O at one atmosphere total pressure: Bulletin of the Earth and Mineral Sciences Experimental Station, The Pennsylvania State University, No. 88, 129p.

Eügster, H. P. and Wones, D. R., 1962, Stability relations of the ferruginous biotite, annite: Journal of Petrology, V. 3, p. 82-125.

Frondel, C. and Baum, J. L., 1974, Structure and mineralogy of the Franklin zinc-iron-manganese deposit, New Jersey: Econ. Geol., V. 69, p. 157-180.

Frondel, C. and Klein, C., 1965, Exsolution in Franklinite: Am. Mineralogist, V. 50, p. 1670-1680.

Haggerty, S. E., 1976, Oxide minerals, Reviews in mineralogy: Mineralogical Society of America, V. 3, 300p.

Hague, J. M., Baum, J. L., Harramann, L. A., and Pickering, R. J., 1956, Geology and structure of the Franklin-Sterling area, New Jersey: G.S.A. Bull., V. 67, p. 435-473.

Kennedy, G. S. and Holser, W. T., 1966, Pressure-volume-temperature and phase relation of water and carbon dioxide: G.S.A.

Lindsley, O.H., 1976, Oxide Minerals, Review in Mineralogy: Mineralogical Society of America, V. 3, 300p.

Mason, B., 1947, Mineralogical aspects of the system Fe_3O_4-Mn_3O_4-$ZnMn_2O_4$-$ZnFe_2O_4$: Am. Mineralogist, V. 32, p. 426-441.

Metsger, R.W., Skinner, B.J., and Barton, P.B., 1969, Structural interpretation of the Sterling Hill ore body, Ogdensburg, N.J.: Geol. Soc. Am. Abs. Prog., Pt. 7, p.150.

Metsger, R.W., Tennant, C.B., and Rodda, J.L., 1958, Geochemistry of the Sterling Hill Zinc deposit, Sussex County, New Jersey: Geol. Soc. Am. Bull., V. 69, p.775-788.

Muller, O., and Roy, R., 1974, The major ternary structural families: New York, Springer-Verlag, 487 p.

Ramdohr, P., 1980, The ore minerals and their intergrowths: New York, Pergamon Press Inc., 1205p.

Ridge, J.D., 1952, Geochemistry of the ores of Franklin, New Jersey: Econ. Geol., V. 47, p. 180-192.

Squiller, S. F., 1976, The geochemistry of franklinite and associated minerals from the Sterling Hill zinc deposit, Sussex County, New Jersey: Lehigh University, M.S. thesis, 231p.

Squiller, S. F. and Sclar, C. B., 1976, Geochemistry of franklinite, willemite, and zincite from the Sterling Hill ore body, N.J.: Geol. Soc. Am. Abs. Prog., V. 8, No. 6.

Stead, R. J., 1980, Progress report on Sherman Fairchild Summer Scholarship: Lehigh University, unpublished.

Takahashi, T. and Myers, C. E., 1963, Nature of the ore forming fluid for the Franklin and Sterling Hill deposits, New Jersey: Symposium: Problems of Postmagmatic ore deposition, Praque, Geol. Survey of Czech., p. 459-465.

Ulmer, G. C., 1971, Research techniques for high pressure and high temperature: New York, Springer-Verlag, 367p.

Whittaker, E. J. W. and Muntus, R., 1970, Ionic radii for use in geochemistry: Geochim. Cosmochim. Acta, V. 34, p. 945-956.

APPENDIX I. Program used for Electron Microprobe Analysis

The following program was used to analyze for Mg, Al, Ti, Fe, Mn, and Zn using the WOS system for point and broad-beam quantitative analysis on the JEOL-733 superprobe. Oxygen was calculated by difference.

```
200, 1 AL
200, 5 >WT O
200, 10 SWITCH BKG OFF
200, 15 EDS 0 10 10
200, 20 PKCNT MG, TI, MN
200, 25 PKCNT AL, FE, ZN
200, 30 RUN ZAF
200, 35 GOTO AL
200, 40 END
```

Element Table

EL	SPEC	XSTAL	POS	BKG OFST	CF	STD INT	BKG INT	BASELN
Mg	ASPEC	TAP	107.51	5.00	0.140	326.28	2.10	0.50
Al	ASPEC	TAP	90.56	5.00	0.274	575.49	4.59	0.50
Ti	BSPEC	LIF	191.29	4.00	0.274	24.14	0.19	0.50
Fe	BSPEC	LIF	134.69	4.00	0.327	90.61	0.88	0.50
Mn	CSPEC	LIF	146.18	4.00	0.035	5.56	0.32	0.50
Zn	SCPEC	LIF	99.70	4.00	0.752	118.67	0.85	0.50
O	ASPEC	STE	65.86	17.00	1.000	10.00	1.00	0.50

EL	WIND	STD
Mg	10.00	Mg
Al	10.00	Al
Ti	10.00	Ti
Fe	10.00	Fe
Mn	10.00	Mn
Zn	10.00	Zn
O	10.00	O

APPENDIX II. Electron Microprobe Analyses

Some of the data presented in this text are averages of a number of data. Individual analysis in atomic percent are presented in this Appendix. All data was corrected for atomic number, absorption affects, and fluorescence, by means of the ZAF correction program presented in Appendix I.

	3-1	3-2	3-3	3-4	3-5
Mg	0.00	0.00	0.03	0.02	0.06
Al	0.00	0.00	1.62	0.91	0.52
Ti	6.44	3.64	10.49	12.47	7.65
Fe	16.95	27.32	10.93	9.11	17.17
Mn	7.38	4.97	12.81	14.38	8.97
Zn	0.51	0.66	0.35	0.45	0.55
O	68.72	63.16	63.78	62.65	65.08
	100.03	100.07	100.10	99.93	99.90

	3-6	3-7	3-8	3-9
Mg	0.00	0.00	0.02	0.06
Al	0.00	0.24	0.00	0.02
Ti	14.70	11.14	7.11	11.17
Fe	3.68	15.86	23.20	5.66
Mn	16.47	11.70	7.27	13.89
Zn	0.44	0.52	0.58	0.33
O	64.71	60.55	61.82	68.87
	100.00	99.89	100.01	100.00

4-1 (average of three analyses)

Mg	0.03	0.00	0.20
Al	0.43	0.21	0.29
Ti	0.14	0.23	0.21
Fe	30.36	30.98	33.32
Mn	0.71	0.70	0.72
Zn	4.00	2.54	1.98
O	64.34	65.34	63.46
	100.01	99.99	100.00

4-2 (average of four analyses)

Mg	0.00	0.00	0.01	0.00
Al	0.88	0.90	0.84	0.78
Ti	0.95	1.21	1.26	1.20
Fe	24.53	24.81	23.79	28.24
Mn	1.70	2.01	1.98	1.97
Zn	10.18	10.61	10.38	10.56
O	61.77	60.46	61.75	62.24
	99.98	100.06	99.99	100.00

APPENDIX II (cont.)

	4-3 (Area, 25x30 μm)	4-4 (Area, 25x30 μm)	4-5 (Area, 25x30 μm)
Mg	0.00	0.00	0.00
Al	0.80	0.89	0.46
Ti	1.08	1.24	1.15
Fe	26.28	25.08	20.50
Mn	1.75	1.87	1.63
Zn	9.21	10.10	5.07
O	60.88	60.82	71.20
	99.98	100.01	100.02

VITA

Albert J. Valentino was born on September 5, 1958 in New York City, the Bronx. His parents are Joseph and Amelia Valentino. In September of 1976 he started his long college career at Herbert H. Lehman College in the Bronx. He later moved to God's Country on his nineteenth birthday where he attended the University of Southern Maine and in May of 1980 was awarded a Bachelor of Arts degree in Geology and the Robert N. Miller geoscience award. In August of 1980 he entered graduate school in the Department of Geological Sciences at Lehigh University where he worked toward his Master of Science degree while he was supported as a graduate teaching assistant. In January of 1983, Mr. Valentino entered the Department of Metallurgy and Materials Engineering at Lehigh University as a graduate research assistant and doctoral candidate to do research on degradation mechanisms in barium titanate dielectrics.

Mr. Valentino is a member of the Geological Society of America, the Mineralogical Society of America, the American Geophysical Union, the American Ceramic Society, and Sigma Xi, the Scientific Research Society.